Groundwater recharge over the past 100 years: regional spatiotemporal assessment and climate change impact over the Saguenay-Lac-Saint-Jean region, Canada

ABSTRACT (max 300 words)

Proper knowledge of potential groundwater recharge (PGR) and its spatiotemporal distribution are essential for sustainable groundwater management, especially within the context of climate change. Here, a robust GIS-based water budget framework was developed to estimate PGR at a regional scale and map its spatial distribution. This framework is demonstrated over the Saguenay-Lac-Saint-Jean region (13,200 km^2) of Quebec (Canada). The PGR mapping process was based on a model incorporating water budget components. The vertical inflows (VI) include water amounts from rainfall and snowmelt, whereby the latter was assessed using HYDROTEL model. VI were combined with the maximum and minimum temperatures to estimate actual evapotranspiration (AET), while the surface runoff (Ru_S) was assessed using the curve number method. Field observations of annual variation in temperatures and the water budget components, over a period of 100 years (1910–2009), were used to provide a comprehensive overview of the effects of climate change on PGR. The last 10 years of the observation period (i.e., 2000-2009) indicate that 6% of the study area have PGR rates of 35–50%. PGR rates of 20–35% occur in 58% of the study area, while 36% have PGR of 5–20%. The trend analysis of temperature time series reveals an average of 1.1±0.6 °C increase over 100 years. Also, an increase in the water budget components is observed. Despite the increasing trends of Ru_S and AET, PGR still showed an increasing trend with an average increase of 0.7±0.4 mm/yr over the past 100 years. This observation indicates that the increase in VI was enough to compensate for the increases in AET and Ru_S. This finding of an increasing PGR in the study area provides useful information for future studies focusing on predicting long-term PGR evolution and for the development of efficient long-term groundwater management strategies.

Keywords
Water budget, Snowmelt, Curve number, GIS, Aquifer, Quebec

Lamine Boumaiza[1,2], Julien Walter[1,2], Romain Chesnaux[1,2], Mélanie Lambert[1,2], Madan Kumar Jha[3], Heike Wanke[4], Andrea Brookfield[5], Okke Batelaan[6], Paulo Galvão[7], Nour-Eddine Laftouhi[8], Christine Stumpp[9]

[1] Département des Sciences appliquées, Université du Québec à Chicoutimi, Saguenay, Québec G7H 2B1, Canada

[2] Centre d'études sur les ressources minérales, Groupe de recherche Risque Ressource Eau, Université du Québec à Chicoutimi, Saguenay, Québec G7H 2B1, Canada

[3] Agricultural and Food Engineering Department, Indian Institute of Technology Kharagpur, West Bengal 721 302, India

[4] Department of Geography and Environmental Management, University of the West of England, Bristol BS16 1QY, United Kingdom

[5] Department of Earth and Environmental Sciences, University of Waterloo, Waterloo, Ontario N2T 0A4, Canada

[6] National Centre for Groundwater Research and Training, College of Science and Engineering, Flinders University, Adelaide, South Australia 5001, Australia

[7] Department of Geology, Federal University of Minas Gerais - Belo Horizonte, Minas Gerais 31270901, Brazil

[8] Faculty of Sciences Semlalia, Cadi Ayyad University, Marrakesh 40000, Morocco

[9] Institute for Soil Physics and Rural Water Management, University of Natural Resources and Life Sciences, Vienna 1190, Austria

1 INTRODUCTION

Groundwater supports ecosystems and anthropogenic activities; and is critical to human health. In recent decades, increased groundwater use and overexploitation has become a serious threat to water security due to rapid deterioration of both groundwater quantity and quality (Kammoun *et al.*, 2018; Seddique *et al.*, 2019; Boumaiza *et al.*, 2020a), and demand for groundwater are expected to continue to increase globally (Achu *et al.*, 2020). The implementation of sustainable groundwater management strategies are required to anticipate and mitigate groundwater deficit scenarios and to sustain or increase current qualities of life. Knowledge of groundwater recharge potential and its distribution (mapping) are necessary for sustainable groundwater management (Ashaolu *et al.*, 2020; Dubois *et al.*, 2021). The groundwater recharge can be defined as the water infiltrating into the subsurface and traveling through the unsaturated zone to reach the water table. Quantifying groundwater recharge remains particularly challenging as it cannot be measured directly (Bredehoeft, 2007; Bakker *et al.*, 2013). The accuracy of groundwater recharge estimate is affected by input parameter uncertainties and/or the neglect or simplification of contributing processes (e.g., lateral flow through the vadose zone). As such, the term “potential groundwater recharge (PGR)” is used in this study to refer to the water amount that is theoretically available to become groundwater recharge. PGR is known to vary spatiotemporally due to variability in catchment landscape, subsurface properties, and meteorological conditions (Healy, 2010; Zomlot *et al.*, 2015). PGR mapping helps to identify the recharge areas for groundwater development, including for identification of areas for artificial PGR (Chowdhury *et al.*, 2010), and is a helpful tool for protecting recharge areas, particularly in areas with expanding urbanization. Urbanization has been linked to changes in quantity and quality of groundwater that can have long-lasting environmental impacts (Cosgrove and Loucks, 2015). PGR mapping also is one of the most important elements in groundwater vulnerability assessment methods, such as the DRASTIC method (Aller *et al.*, 1987).

Many methods have been used to produce PGR maps, using a variety of parameters such as rainfall, lineament features, land slope, drainage pattern, land use/cover, and soil types. These methods include frequency ratio methods (Al-Abadi *et al.*, 2016), random forest models (Golkarian and Rahmati, 2018), decision tree models (Chenini *et al.*, 2010), artificial neural network analyses (Naghibi *et al.*, 2018), evidential belief function approaches (Nampak *et al.*, 2014), and analytical hierarchy process methods (Zghibi *et al.*, 2020). Such methods are usually combined with information provided by perspective-view tools wherein the mapping process is integrated within GIS. These tools, including aerial photographs and near-infrared satellite images, have had limited success due to the absence of spectral resolution (Engman and Gurney, 1991). Still, remote sensing (RS) can be a quick and powerful tool for obtaining spatiotemporal information over a large area, including factors influencing catchment hydrology like geology, geomorphology, land use/cover, and drainage patterns (Jha *et al.*, 2007, 2010; Yeh *et al.*, 2014). GIS provides a support framework to effectively handle large and complex spatial information; it is capable of executing weighted linear combinations based on pixel calculations by integrating multiple thematic layers for site suitability mapping (Wieland and Pittore, 2017; Lentswe and Molwalefhe, 2020). One of the main advantages stemming from integrating RS with GIS within PGR mapping is in the capability to investigate the impacts of climate and catchment landscape on water resources at unprecedented levels of spatiotemporally variability (Batelaan and De Smedt, 2007; Healy, 2010). Most PGR mapping studies, however, have been limited to delineate probable zones of low, moderate, or high PGR, without computing the corresponding PGR rates (Chowdhury *et al.*, 2010; Agarwal and Garg, 2015; Lentswe and Molwalefhe, 2020; Tanveer *et al.*, 2020). Only limited studies have incorporated the spatial distribution of PGR rates. Among them, Batelaan and De Smedt (2007) and Abdollahi *et al.* (2017), who respectively developed seasonal and monthly-based spatially-distributed water balance models for PGR estimation. Wanke *et al.* (2013) adapted a GIS-based process-oriented physically based water balance model to assess the spatial distribution of PGR. Galvão *et al.* (2018) proposed a GIS framework for mapping PGR by incorporating a water budget analysis. There are also an increasing number of studies focused on the long-term temporal variations of PGR due to climate change (Chen *et al.*, 2004; Jyrkama and Sykes, 2007; Woldeamlak *et al.*, 2007; Herrera-Pantoja and Hiscock, 2008; Green *et al.*, 2011; Holman *et al.*, 2012; Taylor *et al.*, 2013; Meixner *et al.*, 2016; Epting *et al.*, 2021), where climate change is found to affect the quantity and distribution of PGR (Ng *et al.*, 2010; Crosbie *et al.*, 2013a, 2013b; Flint and Flint, 2014; El Asri *et al.*, 2019; Busico *et al.*, 2021). While some existing studies are at the global scale (Mohan *et al.*, 2018), regional studies are valuable for identifying potential impact of climate change on sustainable groundwater management.

This review reveals that there are limited studies focusing on mapping the spatial distribution of PGR rates and interpreting the potential impact of climate change on PGR at regional scales. The objective of the present study is to develop and demonstrate a robust and pragmatic GIS-based water budget framework for the evaluation of PGR at regional scale. This newly developed framework will be used to assess and map PGR in the

Saguenay-Lac-Saint-Jean (SLSJ) region of Quebec (Canada). PGR was assessed using a water budget approach, where PGR represents the balance between the captured precipitation and the sum of the runoff and the evapotranspiration. In the present study, meteorological inputs, including rainfall, snowfall accumulated as snowpack, and snowmelt, were considered over a period of 100 years. Additionally, the water budget model is based on spatiotemporal variables for assessing evapotranspiration (i.e., temperature and precipitation), making it relatively easy to adapt to climate and land use change scenarios. The GIS-based water budget framework is demonstrated on the SLSJ region; however, this framework can be applied in other regions of the world. Application to the SLSJ region of Quebec, which is under a humid continental climate, offers unique opportunity to study potentially extreme impacts of climate change as a few degrees of temperature increase would transform snowfall, which makes up over 1/3 of the annual precipitation (as snow water equivalent) to rainfall. Using the developed model, a comprehensive overview of the effect of climate change on PGR is completed from the field observations over a long period of 100 years (1910–2009). This provides a helpful tool for predicting long-term PGR evolution and scientific basis for developing efficient, regional, long-term groundwater management strategies.

2 STUDY AREA

2.1 Location and climate

The study area is the 13,210 km^2 area that makes up the administrative limits of the SLSJ region in the Province of Quebec (Canada) (Figure 1). This region has a humid continental climate with average monthly temperatures ranging from −16 °C in January to +18 °C in July. The mean annual precipitation of 930 mm is uniformly distributed, including a snow water equivalent of 320 mm (Government of Canada, 2021). There is limited water infiltration during winter-early spring seasons (from November to March/April) due to the presence of snowpack acting as a barrier to infiltration. However, the accumulated snowfall during this cold period is intermittingly melting due to occasional increases in temperature before the major snowmelt period generally occurring in April/May. Precipitation in the summer-autumn seasons is mainly in the form of rainfall (Government of Canada, 2021).

2.2 **Geology and hydrogeology**

The basement of the SLSJ region is composed of plutonic felsic to intermediate rocks and a gneissic complex of orthogneiss and paragneiss belonging to the Canadian Precambrian Shield (Laurin and Sharma, 1975; Hébert and Lacoste, 1998). The bedrock that controls the topography is cut by the Phanerozoic Saguenay Graben (Figure 2a), which is approximately 30 km wide. The northern and southern walls of the Saguenay Graben are bounded by trending fault systems (Du Berger *et al.*, 1991) that mark the limits between the lowlands (from 0 m to 200 m above the sea level) and the highlands (up to 1,000 m above sea level) (Figure 2b). The SLSJ region contains two important surface water bodies, Saint-Jean Lake and the Saguenay River which is a tributary of the Saint-Lawrence River. Around Saint-Jean Lake and in the lowland areas, there are several remnants of an Ordovician platform composed of a series of stratified sedimentary rocks, including siliciclastic strata, micritic limestones, and highly fossiliferous alternating limestones and shales. A maximum thickness of 110 m has been recorded in the Ordovician sequence (CERM-PACES, 2013). Limestones occur along the northern, western and southern shores of Saint-Jean Lake and are separated from the Saguenay outcrops by approximately 45 km of Precambrian rocks (Desbiens and Lesperance, 1989). The SLSJ region was marked by the last glaciation event, which began approximately 85,000 years ago —during the early stage of the Wisconsinan period— and ended around 7,000 years ago (Parent and Occhietti, 1988). During its retreat towards the west-northwest, the last glacier covering the SLSJ region left a discontinuous and heterogeneous layer of till, several terminal moraines, glaciolacustrine deposits and fluvioglacial esker deposits (Lasalle and Tremblay, 1978; Daigneault *et al.*, 2011). Following the glacier retreat, approximately 11,800 years ago, the lowlands of the SLSJ region were part of the Laflamme Sea, leading to the deposition of a semi-continuous extensive layer of laminated clayey silt and gray silty clay. The regional Saguenay Graben has been marked by large accumulations of Quaternary deposits. Those deposits mainly include sand, gravel, and clay-silt (Figure 2c); they have a thickness of up to 180 m in the central SLSJ lowlands (Dionne and Laverdière, 1969; Lasalle and Tremblay, 1978).

Several hydrogeological systems were created through the geological evolution of the SLSJ region. Fluvioglacial sediments are the most productive regional aquifers and are consequently favoured as a source for municipal drinking water. They are frequently covered by regional marine clay aquitards forming the confined aquifer systems of the SLSJ region (Dessureault, 1975; CERM-PACES, 2013), but also have unconfined regions, such as the major valleys of the highlands, which were not covered by the fine sediments from the Laflamme Sea. Confined and unconfined aquifers occur both in the fractured rock and Pleistocene deposits and combine locally to form multilayered aquifers with unconnected and interconnected parts (Chesnaux *et al.*, 2012; CERM-PACES, 2013; Richard *et al.*, 2014; Walter *et al.*, 2017). The interconnection could be natural and related to the presence of fractures in the top layer of the bedrock (Chesnaux and Elliott, 2011), or could be due to defective borehole seals at the interface between the bedrock and the granular aquifer (Richard *et al.*, 2013). In the highlands, water infiltrates into a network of interconnected fractures and faults within igneous and metamorphic rocks. The groundwater systems present in the highlands and lowlands primarily discharge into Saint-Jean Lake and the Saguenay River (Meinken and Stober, 1997; Walter *et al.*, 2017).

3 MATERIALS AND METHODS

3.1 Data source

The regional hydrogeology of the SLSJ region is well defined due to the Quebec's governmental PACES program (*Programme d'acquisition de connaissances sur les eaux souterraines*) (Figure 1). The PACES-SLSJ program included diverse hydrogeology studies aiming to investigate the hydraulic connections between bedrock aquifers and overlying granular aquifers; to assess numerically the groundwater travel-time through the vadose zone; to quantify local PGR; to develop alternatives for understanding the vulnerability of regional aquifers to contamination; to document aquifer properties; to characterize the internal architecture of granular aquifers; and to study the regional groundwater chemical evolution (Chesnaux *et al.*, 2011; Richard *et al.*, 2014, 2016b, 2016a; Boumaiza *et al.*, 2015, 2017, 2019, 2020c, 2020b, 2021a, 2021b; Walter *et al.*, 2017, 2018, 2019; Ferroud *et al.*, 2019; Chesnaux and Stumpp, 2018; Ferroud *et al.*, 2018; Labrecque *et al.*, 2020). One of the main products of the multi-faceted PACES-SLSJ projects was the development of a comprehensive regional-scale database including: (i) technical details on the groundwater sampling points (observation wells, private wells, municipal wells) such as location, depth, stratigraphy and diameter; (ii) groundwater physicochemical results; (iii) static groundwater level; (iv) subsurface materials and surficial soils; (v) land-use, and (vi) topography over the SLSJ region (CERM-PACES, 2013). Information from this database was used in the present study.

3.2 Assessment of potential groundwater recharge

In this study, the PGR was calculated using a water budget approach. PGR refers to the amount of water that is theoretically available to become recharge, neglecting the amounts that may flow horizontally through the vadose zone without reaching the water table. The principle of water budget approach (Steenhuis and Van Der Molen, 1986) is that the difference between the input and output fluxes of water in the aquifer system is equal to the change in water storage. This method is one of the most common methods used for large-scale PGR assessment (Yeh *et al.*, 2007; Tilahun and Merkel, 2009; Huet *et al.*, 2016; Galvão *et al.*, 2018). PGR was estimated using Equation 1, where VI is the estimated vertical inflow from rainfall and/or snowmelt, Ru_S is surface runoff, and AET is actual evapotranspiration.

$$PGR = VI - (Ru_S + AET) \tag{1}$$

Figure 3 shows the method followed in the present study for computing PGR. The subsections below describe the approaches used for estimating each of the water budget components. The calculations of VI, AET, and Ru_S were used to produce the relative maps of VI, AET, and Ru_S; the latter were combined to generate the annual PGR maps. The processing was automated in ArcGIS program (ESRI, 2019).

3.2.1 Estimation of vertical inflows

The vertical inflows (VI) data were assessed from climate stations operated by the Quebec Ministry of the Environment (*Ministère de l'Environnement et de la Lutte contre les Changements Climatiques*, MELCC). To maximize spatial coverage over the Province, data collected from climate stations operated by Hydro-Quebec and Alcan RioTinto have been included. A total of 22 climate stations, distributed almost evenly over the entire SLSJ region (Figure 4), were considered (Poirier *et al.*, 2014). In the present study, VI is defined as the sum of rainfall and the water equivalent derived from snowmelt. These estimates were provided by the *Centre d'expertise hydrique du Québec* (CEHQ), wherein the physically-based distributed hydrological model HYDROTEL (Fortin *et al.*, 1995, 2007) has been used to compute the water equivalent derived from snowmelt over the Province. This hydrological model has been successfully applied in various Southern Canada watersheds (Turcotte *et al.*, 2007; Huet *et al.*, 2016). VI data estimated at climate stations were interpolated by isotropic kriging and provided by CEHQ under gridded distribution form representing the observation points (Figure 4). These data were generated on daily time intervals over a period of 100 years (1910–2009), with 165 interpolated observation points over the SLSJ region (Figure 4).

3.2.2 ***Estimation of surface runoff***

Estimates of Ru_S were based on the Soil Conservation Service/Curve Number (SCS/CN) method (Cronshey, 1986). This method, initially proposed by the US Department of Agriculture, was derived from flood modeling and has been adopted by many hydrological models including SWAT (Gassman *et al.*, 2007). The SCS/CN method relates runoff to precipitation by assuming that for a given precipitation event, all water amount exceeding the soil infiltration capacity would contribute to Ru_S. The SCS/CN method integrates terrain characteristics including type of soil, land-use, and slope, and has been widely used to estimate Ru_S (Anbazhagan *et al.*, 2005; Deshmukh *et al.*, 2013; Satheeshkumar *et al.*, 2017; El Garouani *et al.*, 2020). Previous research has demonstrated that it can match conditions in humid continental regions of Quebec (Monfet, 1979; Huet *et al.*, 2016). In the present study, information on terrain characteristics was available from CERM-PACES (2013). Using the SCS/CN method, the Ru_S was estimated using Equation 2 proposed by Cronshey (1986), and modified for regional spring snowmelt conditions following Woodward *et al.* (2003); Lim *et al.* (2006); Yuan *et al.* (2014); Huet *et al.* (2016). S is the retention parameter expressed in mm/d; and can be calculated using Equation 3 where CN is the curve number determined by land use/cover characteristics. The CN value is determined daily to reflect changes in soil moisture conditions at the observation point locations (Figure 4) following the method summarized in Figure 5 and described below.

$$Ru_s = \frac{(VI - 0.01S)^2}{VI + 0.99S} \quad \text{With VI} > 0.01S \tag{2}$$

$$S = \frac{25400}{CN} - 254 \tag{3}$$

Phase I includes four steps, where Step 1 consists of identifying the main different soil type observed at the location. Based on the SLSJ surface deposits (Figure 6a) (CERM-PACES, 2013), the main observed soil types were codified according to Geological Survey of Canada codification (Table 1) (Parent *et al.*, 2010). In Step 2 the soil types are grouped according to water infiltration capacity. Four groups were proposed, classified 1 to 4 and reflecting decreasing water infiltration capacity (Table 2). For example, group 1 regroups sediments with high water infiltration capacity. Therefore, group 1 would have lower runoff compared to group 4, which would have sediments with a low water infiltration capacity such as rock, clay, and till, that would be more favorable for runoff. Figure 6b shows the distribution of the four established water infiltration capacity groups over the study area. Step 3 of Phase I (Figure 5) specifies the land-use at the observation points shown in Figure 4. The comprehensive map of the land-use characteristics over the SLSJ region (Figure 6c) (CERM-PACES, 2013) indicates four dominant land use types: (i) forest (68%), (ii) agricultural (16%), (iii) urban (1%), and (iv) water bodies (15%). Step 4 of Phase I (Figure 5) consists of identifying the terrain slope as the value of runoff potential is affected by topography (Figure 6d) (CERM-PACES, 2013). Four terrain slope categories were established, areas with a slope of (i) <3%, (ii) 3-8%, (iii) 8–15%, and (iv) >15%. Table 3 presents the CN_i values, which can be determined according to type of soil, land-use, and slope of terrain. A low CN_i value corresponds to a low runoff capacity, whereas a high CN_i value indicates a high runoff capacity. Similarly to the study of Huet *et al.* (2016), it was assumed that if the slope is >15%, independent of the type of soil and land-use, there would be maximum runoff, i.e. $CN_i = 90$.

For Phase II in Figure 5, step 1 calculates the antecedent precipitation index (API) to determine the antecedent moisture conditions (AMC). The API considers the cumulative amount of VI (in mm) throughout the 14 days preceding the day of interest, calculated using Equation 4 (Monfet, 1979). Once the API is calculated, the chart shown in Figure 7 can be used to determine the AMC class (class I, II or III) by specifying the corresponding time-period of the day of interest (Step 2 of Phase II; Figure 5).

$$\mathrm{API} = \sum_{i=1}^{n=14} 0.85^{i} \cdot \mathrm{VI}_i \qquad (4)$$

Once the AMC class is identified, the CN_i is then modified according to the determined AMC class. However, no modification of CN_i is required if an event is categorized as AMC II (AMC class I, II and III are determined from y-axis of the chart shown in Figure 7). Otherwise, the conversion of the CN_i to CN is based on Equations 5 and 6 (Cronshey, 1986). Maps of soil type, topography, and land-use, which were required to determine CN_i, were available in raster format allowing for the creation of CN_i maps which were fixed in time. The daily CN_i maps were combined with AMC to establish the CN daily maps and were subsequently used to create the daily Retention parameter (S) maps according to Equation 3. The spatially-distributed daily VI were then combined with the spatially-distributed daily S data (Equation 2) to estimate daily spatially-distributed Ru_S and produce the relative daily Ru_S maps.

$$\text{For AMC I: } CN = \frac{4.2\ CN_i}{10 - 0.058\ CN_i} \tag{5}$$

$$\text{For AMC III: } CN = \frac{23\ CN_i}{10 + 0.13\ CN_i} \tag{6}$$

3.2.3 ***Estimation of actual evapotranspiration***

To estimate AET, the PET was first calculated using the empirical equation developed by Bisson and Roberge (1983). This equation (Equation 7) is adapted to the northern climate conditions in Quebec (Dionne *et al.*, 2008), and uses the daily maximum temperature (T_{Max}) and daily minimum temperature (T_{Min}). The T_{Max} and T_{Min} (in °C) were provided by CEHQ, for each observation point (Figure 4), under vectorial formats on a 0.1° longitude and latitude grid. The temperature data were then interpolated by a tension spline approach to obtain a new raster for each pixel (250 m × 250 m). This daily PET was then used to calculate the annual PET. Using the annual PET, the annual AET was calculated using

Equation 8 (Budyko, 1974), in which annual VI was introduced. A raster of the annual VI (250 m × 250 m) was created using a tension spline interpolation of CEHQ data over the study area. Equation 8 was used in this study because it has proven to provide accurate estimates of AET in numerous studies (Zhang *et al.*, 2001; Oudin, 2004; Huet *et al.*, 2016).

$$\mathrm{PET} = 0.029718\ (\mathrm{T_{Max}} - \mathrm{T_{Min}})\ .\ e^{0.019\left[\frac{9}{5}\,(\mathrm{T_{Max}} + \mathrm{T_{Min}}) + 64\right]} \tag{7}$$

$$\mathrm{AET} = \left[\mathrm{VI}\ .\ \left(1 - \exp^{\left(-\frac{\mathrm{PET}}{\mathrm{VI}}\right)}\right)\ .\ \mathrm{PET}\ .\ \tanh\left(\frac{\mathrm{VI}}{\mathrm{PET}}\right)\right]^{0.5} \tag{8}$$

3.3 Variability of potential groundwater recharge under climate change

The change in temperature, water budget components (VI, AET, and Ru_S) and PGR was estimated for the period 1910–2009. Five observation points, distributed evenly over the entire study area, were selected. Two observation points (O.P.#1 and #4) are in the highland areas, while other three observation points (O.P.#2, #3, and #5) are in the lowland areas (Figure 8d). Trend lines (linear regression lines corresponding to data series) were calculated, and the Mann-Kendall test (Mann, 1945; Kendall, 1975) was used to evaluate the trend tendency of each data series using XLSTAT software (Addinsoft, 2021). The null hypothesis (H_0) for the Mann–Kendall test indicates no trend, whereas the alternative hypothesis (H_a) indicates either an upward or downward trend. Positive Kendall's Ʈ corresponds to an upward trend, while negative Kendall's Ʈ indicates a downward trend (Pohlert, 2020).

4 RESULTS

To understand the spatial distribution of PGR over the SLSJ region, it is useful to first analyze the spatial distribution of the water budget components, VI, AET and Ru_S. The subsections below describe the spatial distribution of each water budget component from the last 10 years of the observation period followed by a description of their temporal variation.

4.1 Spatial distribution of mean vertical inflows 2000–2009

The VI rates vary between 800 and 1075 mm/yr (Figure 8a). Higher VI rates ranging (900–1075 mm/yr) occupy 70% of the study area and were primarily observed (i) along the northern band of the study area from Saint-Fulgence to Dolbeau-Mistassini; (ii) over some of the southeast area including the Chicoutimi and La Baie portion; and (iii) along the southwest sector of the study area that includes Lac-Bouchette (Figure 8a). Lower VI rates (800–900 mm/yr) occupy 30% of the study area and were found at (i) the extreme eastern portion, (ii) the central southern band relative to Saguenay River including Jonquière and Lac-Kénogami, and (iii) the northwestern sector from Dolbeau-Mistassini to Roberval (Figure 8a).

4.2 Spatial distribution of mean actual evapotranspiration 2000–2009

Figure 8b shows the spatial distribution of the mean AET over the study area. The AET rates vary between 475 and 590 mm/yr. The highest AET rates (550–590 mm/yr), occupying 46 % of the study area, were observed (i) along the northern band of the study area from Saint-Fulgence sector at the northeast to the sector of Dolbeau-Mistassini at the northwest; (ii) over the La Baie sector at southeast portion; and (iii) at Lac-Bouchette sector located at the southwest of the area (Figure 8b). The AET rates lower than 550 mm/yr, occupying 54 % of the study area, were mainly observed (i) at the extreme eastern part; and (ii) at the southern band relative to Saguenay River from Chicoutimi to Alma sector and over the southern band relative to Saint-Jean Lake from Alma to Saint-Félicien sector

(Figure 8b). High AET rates overall correspond to areas with high VI and thus potentially higher water availability, while the areas featuring lower AET rates correspond to areas experiencing low VI. This is also related to the nature of the Equation 8 used for assessing AET, which is based on PET considering VI in addition to T_{Max} and T_{Min}.

4.3 Spatial distribution of mean surface runoff 2000–2009

Ru_S ranges from 6 to 350 mm/yr over the study area (Figure 8c). The north-eastern and the eastern parts of the study area (40% of the study area) was mainly dominated by high Ru_S rates (200–350 mm/yr), while the rest (60%) of the study area was dominated by Ru_S rates lower than 200 mm/yr (Figure 8c). High Ru_S rates were related areas with rock outcrops on the ground surface (CERM-PACES 2013), and are characterized by the steepest slopes (Figure 6d), both limiting the water infiltration process. Low Ru_S rates are related to the granular deposits dominating ground surface with modest slopes (CERM-PACES 2013) that allow water to infiltrate into the subsurface and subsequently limit the runoff (Figure 6d).

4.4 Spatial distribution of mean potential groundwater recharge 2000–2009

PGR rates were found to spatially vary from 50 to 515 mm/yr (Figure 8d). The sectors having highest rates of PGR with 350–515 mm/yr (35–50% of VI) occupy only 6% of the study domain and were mainly observed in the northern band from Saint-Fulgence sector to the sector located at the north of Alma (Figure 8d). Areas located at the northern part of Lac-Bouchette and a small region located in the southern part of La Baie area also were identified with some of the highest rates of PGR (Figure 8d). The areas identified with highest rates of PGR were mainly characterized by higher VI rates (Figure 8a), lower runoff rates (Figure 8c), granular deposits (Figure 6b), and modest land-slopes (<8%) (Figure 6d).

All these characteristics are in favor for infiltration of water into the subsurface. The effect of the highest rates of AET (northern band of the study area) on PGR rates appears to be insignificant, due to the higher VI captured here in combination with lower runoff. Areas with PGR rates ranging from 200–350 mm/yr, corresponding to 20–35% of VI, occupy approximately 58% of the study area and are distributed evenly over the entire study area. Areas showing PGR rates <200 mm/yr —including regions with 50–150 and 150–200 mm/yr corresponding respectively to mean PGR rates of 5–15 and 15–20% of VI— occupy approximately 36% of the study area. They are distributed in scattered areas across the domain in addition to a larger area in the eastern part of the study area. Even though this eastern part is under forest cover with normally expected high water infiltration, it was found to have moderate VI (Figure 8a) and high runoff rates (Figure 8c) due to steepest slopes of rock outcrops limiting the water infiltration process.

4.5 **Temporal variation in water budget components**

A clear increase in the average temperature was visually observed (Figure 9a) and confirmed with positive Kendall's Ʈ (p-value <0.05) over all the five observation points (O.P.#1 to O.P.#5) (Table 4). The temperature trends indicate an increase of 1.1 °C over 100 years at the study area. The five observation points show a continuous increase in VI (Figure 9b) with an average trend of 165 mm over 100 years (1.65 mm/yr) (positive Kendall's Ʈ with p-value <0.05 were calculated from VI data – Table 4). The Ru_S quantities were also observed to increase over the time at the five observation points (Figure 9c), however, the Mann-Kandel results (Table 4) indicate that trends in Ru_S at O.P.#3 and O.P.#4 were not statistically significant (p-value = 0.121 and 0.755 respectively; Figure 9c). O.P.#4 is located in a forest area (Figure 6c) with slopes <3% (Figure 6d) resulting in

VI dominated over runoff. In addition, the terrain at O.P.#4 is covered by granular deposits of group #1 (Figure 6b), having sediments with high water infiltration capacity and consequently low Ru_S. The observed increase in temperature resulted in a statistically significant increasing trend in AET at all the observation points O.P.#1 to O.P.#5 (Figure 9d; Table 4). The mean annual PGR rates over 100 years also have a statistically significant increasing trend at all five observation points (Figure 10; Table 4), where the average increase in PGR was 0.7±0.4 mm/yr. This increase in PGR is consistent with expectations for Eastern North America which received more precipitation with time, resulting in an increase in an PGR (Rivard *et al.*, 2014; Lindquist *et al.*, 2019; Atawneh *et al.*, 2021).

5 DISCUSSION

5.1 Potential groundwater recharge map

In the study area, highest rates of PGR correspond to areas with forest and agricultural land use. These types of land use promote water infiltration more than urban areas with impermeable surfaces which direct the VI into runoff rather than infiltration (Baier *et al.*, 2014; Wakode *et al.*, 2018). The PGR rates for SLSJ region vary from 5 to 515 mm/yr (5–50 % of annual VI), and are consistent with small-scale studies in the SLSJ region using other methods for estimating PGR. Boumaiza et al. (2020b) used stable isotopes to estimate PGR at Saint-Honoré aquifer in the SLSJ region and found PGR rates of 292 mm for the winter-spring period and 274 mm for the summer-autumn period, providing thus an average annual PGR rate of 566 mm. This 2018/2019 average PGR rate is comparable to that estimated for the same region in this work, ranging from 400–515 mm/yr. For the Saint-Honoré aquifer, Labrecque *et al.* (2020) found a PGR rate of 350 mm/yr in 2017 (35% of annual precipitation) using the water table fluctuation method. This 2017 PGR rate is somewhat lower than the 2000–2009 PGR interval determined in the present study (400–515 mm/yr) likely due to a difference in the time period and method applied. Specifically, the water table measurements used to estimate recharge as part of the water table fluctuation method can be significantly affected by other factors, such as water pumping, deep groundwater flow, hydraulic connections between aquifers, and lake discharge (Halford and Mayer, 2000; Scanlon *et al.*, 2002; Stephens, 2009).

The accuracy of estimating PGR is directly dependent on the uncertainties in each of the water budget method components, i.e., VI, AET and Ru_S. Uncertainty in the HYDROTEL derived VI are often due to the wind issues, which can both prevent or contribute snow from being naturally captured by the snow gauges. However, uncertainties related to the wind effect are expected to be low as most operational agencies, including CEHQ, use snow surveys to correct snow water equivalent values throughout the winter season. The AET was derived from the PET, which relies solely on temperature and VI. Some of the uncertainties regarding the AET estimates can be related to the simplification of the approach which does not consider important AET factors such as soil moisture or air vapour saturation. If these observations were available, a more complex approach for estimating AET could be implemented using an energy budget (Dubois *et al.*, 2021). The SCS/CN method has received some criticism related mostly to its empirical origin developed for specific US context (Ponce and Hawkins, 1996; Ogden *et al.*, 2017). However, this method has been continuously adapted to new environments (Monfet, 1979; Miliani *et al.*, 2011; Deshmukh *et al.*, 2013; Bartlett *et al.*, 2016; Ross *et al.*, 2018).

5.2 **Long-term trend of water budget components**

The observed increase in temperature of 1.1 °C over the study area is comparable to that presented by Ouranos (2015), who found that the SLSJ region marked an increase in temperature about 1.1–2 °C over 62 years (1950–2011). In the present study, the increase of the average temperature for the study area was observed to be accompanied by an increase of VI amounts. Among the main consequences of climate change on precipitation regimes is the fact that warmer air can hold more moisture and that the amount of water vapor —transported from the tropics to higher latitudes— is significantly increased. This water transport contributes to decreasing precipitation in drier regions, and inversely, contributes to increasing precipitation in humid continental regions such as the case of the Province of Quebec (Held and Soden, 2006; Ouranos, 2015). Warming global temperatures can lead to increases in extreme precipitation events that can subsequently increase surface runoff from soils unable to absorb heavy rainfall and/or snowmelt (e.g., Shultz ,2020), which is consistent with the increasing trends in Ru_s observed in this study.

The annual increase in PGR simulated in this study for the is consistent with the results from the PGR study conducted by Dubois *et al.* (2021) in the Montreal region of Southern Quebec. In this comparable study, Dubois *et al.* (2021) found that PGR presented a statistically significant increasing trend over 56 years (1961–2017). In this study, O.P.#4 shows a steep increase in PGR rates, whereas O.P.#1 shows the most modest increase in PGR rates. At O.P.#4 the lower rates of runoff (Figure 9c) contribute to elevated rates of PGR. Conversely, O.P.#1 was observed to capture low VI, the highest rates of runoff, and the moderate rates of AET over the time; these features contribute to having modest increase in PGR at O.P.#1. Interestingly, the PGR rates marked an increasing trend over time, at the five observation points (Figure 10), despite (i) the increasing trends of the AET, (ii) the increasing trend of Ru_S over 100 years, and (iii) the overall statistically significant increases in temperature. These observations indicate that the increase in VI can compensate for the increases in AET and Ru_S. The overall annual variability in PGR over time is linked to that of temperature and VI. Here, the observed relationships between PGR, VI and temperature patterns are consistent with that reported in other studies undertaken under similar climate conditions and comparable geological environments (Hayashi and Farrow, 2014; Chemingui *et al.*, 2015; Dubois *et al.*, 2021).

6 CONCLUSION

In this study, a GIS-based distributed water budget method was developed to map the spatial distribution of PGR over the SLSJ region of Quebec experiencing seasonally variable meteorological inputs. Temporal variations in PGR were identified over the past 100 years (1910–2009); allowing evaluation of the effect of climate change on PGR. Results show that the 2000–2009 average PGR rates over the SLSJ region vary from 5 to 515 mm/yr corresponding to average PGR rates of 5–50% of the annual VI. The areas identified with the highest PGR featured higher VI rates and lower runoff rates and were dominated by granular deposits with high infiltration capacity and have modest land-slopes (<8%). The preferential PGR areas are essential for the quantitative replenishment of groundwater resources. However, they are potentially most vulnerable to surficial contamination, and consequently, they should be carefully managed.

Changes in water budget components over the time were estimated. An increase in average temperature was observed through the time with an average of +1.1±0.6 °C increase over 100 years. The average annual PGR rates showed an increasing trend with an average increase of 0.7±0.4 mm/yr. The PGR rates marked an increasing trend despite (i) the increase of AET, (ii) the increase of Ru_S, and (iii) the increase in temperature. These observations indicate that the increase in VI was enough to compensate for the increases in AET and Ru_S. Such observations are aligned with what was expected as an increase of PGR for Eastern North-America, and results of this study are consistent with other localized studies, demonstrating the ability of the GIS-based water balance approach used to simulate representative estimates of PGR.

Results of this work demonstrate how this approach can be used to predict long-term PGR evolution and find the key factors influencing groundwater resources. It can support the development of efficient long-term groundwater management strategies under climate change. The SLSJ regional PGR map is a helpful tool for evaluating the vulnerability of SLSJ aquifers to contamination when combined with the DRASTIC index approach. Validation of the increasing of PGR trend over the time is recommended through continued monitoring of water levels in this region. At present, no long-term data sets of water table level fluctuations for the region are available. In addition, investigations related to other factors affecting PGR, such as the role of soil moisture and groundwater in AET, would improve the estimates of PGR using the GIS-based framework demonstrated here.

Data availability statement

The data supporting the findings of this study are available from the Figures 6, 8, 9 and 10 of this manuscript.

Acknowledgments

The authors would like to thank the Natural Sciences and Engineering Research Council of Canada for funding this project (Grant Nr. RGPIN-2020-04721).

REFERENCES

Abdollahi K, Bashir I, Verbeiren B, Harouna MR, Van Griensven A, Huysmans M, Batelaan O. 2017. A distributed monthly water balance model: formulation and application on Black Volta Basin. *Environmental Earth Sciences* **76** (198): 1–18

Achu AL, Reghunath R, Thomas J. 2020. Mapping of Groundwater Recharge Potential Zones and Identification of Suitable Site-Specific Recharge Mechanisms in a Tropical River Basin. *Earth Systems and Environment* **4** (1): 131–145

Addinsoft. 2021. *XLSTAT statistical and data analysis solution*. New York, USA. https ://www.xlsta t.com.

Agarwal R, Garg PK. 2015. Remote Sensing and GIS Based Groundwater Potential & Recharge Zones Mapping Using Multi-Criteria Decision Making Technique. *Water Resources Management* **30** (1): 243–260

Al-Abadi AM, Al-Temmeme AA, Al-Ghanimy MA. 2016. A GIS-based combining of frequency ratio and index of entropy approaches for mapping groundwater availability zones at Badra–Al Al-Gharbi–Teeb areas, Iraq. *Sustainable Water Resources Management* **2** (3): 265–283

Aller L, Bennett T, Lehr JH, Petty RJ, Hackett G. 1987. *DRASTIC : A Standardized Method for Evaluating Ground Water Pollution Potential Using Hydrogeologic Settings*. Doc. EPA/600/2-87/035. United States Environmental Protection Agency (USEPA), Washington, DC.

Anbazhagan S, Ramasamy SM, Das Gupta S. 2005. Remote sensing and GIS for artificial recharge study, runoff estimation and planning in Ayyar basin, Tamil Nadu, India. *Environmental Geology* **48** (2): 158–170

Ashaolu ED, Olorunfemi JF, Ifabiyi IP, Abdollahi K, Batelaan O. 2020. Spatial and temporal recharge estimation of the basement complex in Nigeria, West Africa. *Journal of Hydrology: Regional Studies* **27** (100658): 1–19

El Asri H, Larabi A, Faouzi M. 2019. Climate change projections in the Ghis-Nekkor region of Morocco and potential impact on groundwater recharge. *Theoretical and Applied Climatology* **138**: 713–727

Atawneh DA, Cartwright N, Bertone E. 2021. Climate change and its impact on the projected values of groundwater recharge: a review. *Journal of Hydrology* DOI: https://doi.org/10.1016/ j.jhydrol.2021.126602

Baier K, Schmitz KS, Azzam R, Strohschoen R. 2014. Management Tools for Sustainable Ground Water Protection in Mega Urban Areas-Small Scale Land use and Ground Water Vulnerability Analyses in Guangzhou, China. *International Journal of Environmental Research* **8** (2): 249–262

Bakker M, Bartholomeus R, Ferre T. 2013. Groundwater recharge: processes and quantification. *Hydrology and Earth System Sciences* **17**: 2653–2655

Bartlett MS, Parolari AJ, McDonnell JJ, Porporato A. 2016. Beyond the SCS-CN method: A theoretical framework for spatially lumped rainfall-runoff response. *Water Resource Research* **52** (6): 4608–4627

Batelaan O, De Smedt F. 2007. GIS-based recharge estimation by coupling surface-subsurface water balances. *Journal of Hydrology* **337** (3–4): 337–355

Du Berger R, Roy DW, Lamontagne M, Woussen G, North RG, Wetmiller RG. 1991. The Saguenay (Quebec) earthquake of November 25, 1988: seismologic data and geologic setting. *Tectonophysics* **186**: 59–74

Bisson J, Roberge F. 1983. *Prévision des apports naturels: Expérience d'Hydro-Québec*. Workshop on flow predictions. Toronto: Institute of Electrical and Electronics Engineers (IEEE).

Boumaiza L, Chesnaux R, Drias T, Walter J, Huneau F, Garel E, Knoeller K, Stumpp C. 2020a. Identifying groundwater degradation sources in a Mediterranean coastal area experiencing significant multi-origin stresses. *Science of The Total Environment* **746** (141203): 1–20

Boumaiza L, Chesnaux R, Walter J, Meghnefi F. 2021a. Assessing response times of an alluvial aquifer experiencing seasonally variable meteorological inputs. *Groundwater for Sustainable Development* **14** (100647): 1–12 DOI: doi.org/10.1016/j.gsd.2021.100647

Boumaiza L, Chesnaux R, Walter J, Stumpp C. 2020b. Constraining a flow model with field measurements to assess water transit time through a vadose zone. *Groundwater* DOI: doi.org/10.1111/gwat.13056

Boumaiza L, Chesnaux R, Walter J, Stumpp C. 2020c. Assessing groundwater recharge and transpiration in a humid northern region dominated by snowmelt using vadose-zone depth profiles. *Hydrogeology Journal* **28** (7): 2315–2329

Boumaiza L, Rouleau A, Cousineau PA. 2015. Estimation de la conductivité hydraulique et de la porosité des lithofaciès identifiés dans les dépôts granulaires du paléodelta de la rivière Valin dans la région du Saguenay au Québec. In *Proceedings of the 68th Canadian Geotechnical Conference, Quebec City, Quebec, Canada*9.

Boumaiza L, Rouleau A, Cousineau PA. 2017. Determining hydrofacies in granular deposits of the Valin River paleodelta in the Saguenay region of Quebec. In *Proceedings of the 70th Canadian Geotechnical Conference and the 12th Joint CGS/IAH-CNC Groundwater Conference, Ottawa, Ontario, Canada*8.

Boumaiza L, Rouleau A, Cousineau PA. 2019. Combining shallow hydrogeological characterization with borehole data for determining hydrofacies in the Valin River paleodelta. In *Proceedings of the 72nd Canadian Geotechnical Conference, St-John's, Newfoundland, Canada.*8.

Boumaiza L, Walter J, Chesnaux R, Karthikeyan B, Lakshmanan E, Rouleau A, Wachniew P, Stumpp C. 2021b. An operational methodology for determining relevant DRASTIC factors and their relative weights in the assessment of aquifer vulnerability to contamination. *Environmental Earth Sciences* **80** (281): 1–19 DOI: doi.org/10.1007/s12665-021-09575-w

Bredehoeft J. 2007. It is the discharge. *Ground Water* **45** (5): 523–523

Budyko MI. 1974. *Climate and Life*. International Geophysical Series, 18. Academic Press, New York.

Busico G, Ntona MM, Carvalho SCP, Patrikaki O, Voudouris K, Kazakis N. 2021.

Simulating future groundwater recharge in coastal and inland catchments. *Water Resources Management* DOI: doi.org/10.1007/s11269-021-02907-2
CERM-PACES. 2013. *Résultats du programme d'acquisition de connaissances sur les eaux souterraines de la région Saguenay-Lac-Saint-Jean*. Centre d'études sur les ressources minérales, Université du Québec à Chicoutimi.
Chemingui A, Sulis M, Paniconi C. 2015. An assessment of recharge estimates from stream and well data and from a coupled surface-water/groundwater model for the des Anglais catchment, Quebec (Canada). *Hydrogeology Journal* **23** (8): 1731–1743
Chen Z, Grasby SE, Osadetz KG. 2004. Relation between climate variability and groundwater levels in the upper carbonate aquifer, southern Manitoba, Canada. *Journal of Hydrology* **290**: 43–62
Chenini I, Ben Mammou A, El-May M. 2010. Groundwater recharge zone mapping using GIS-based multi-criteria analysis: A case study in Central Tunisia (Maknassy Basin). *Water Resources Management* **24**: 921–939
Chesnaux R, Elliott AP. 2011. Demonstrating evidence of hydraulic connections between granular aquifers and fractured rock aquifers. In *Proceedings of GeoHydro 2011, Joint Meeting of the Canadian Quaternary Association and the Canadian Chapter of the International Association of Hydrogeologists, August 28–31, 2011, Quebec City, Quebec, Canada*8.
Chesnaux R, Stumpp C. 2018. Advantages and challenges of using soil water isotopes to assess groundwater recharge dominated by snowmelt at a field study located in Canada. *Hydrological Sciences Journal* **63** (5): 679–695
Chesnaux R, Lambert M, Walter J, Fillastre U, Hay M, Rouleau A, Daigneault R, Moisan A, Germaneau D. 2011. Building a geodatabase for mapping hydrogeological features and 3D modeling of groundwater systems: Application to the Saguenay-Lac-St.-Jean region, Canada. *Computers and Geosciences* **37** (11): 1870–1882
Chesnaux R, Rafini S, Elliott AP. 2012. A numerical investigation to illustrate the consequences of hydraulic connections between granular and fractured-rock aquifers. *Hydrogeology Journal* **20** (8): 1669–1680
Chowdhury A, Jha MK, Chowdary VM. 2010. Delineation of groundwater recharge zones and identification of artificial recharge sites in West Medinipur district, West Bengal, using RS, GIS and MCDM techniques. *Environmental Earth Sciences* **59** (6): 1209–1222
Cosgrove WJ, Loucks DP. 2015. Water management: Current and future challenges and research directions. *Water Resources Research* **51**: 4823–4839
Cronshey R. 1986. *Urban hydrology for small watersheds*. US Dept. of Agriculture, Soil Conservation Service, Engineering Division. Technical Release 55.
Crosbie RS, Pickett T, Mpelasoka FS, Hodgson G, Charles SP, Barron OV. 2013a. An assessment of the climate change impacts on groundwater recharge at a continental scale using a probabilistic approach with an ensemble of GCMs. *Climatic Change* **117** (1–2): 41–53
Crosbie RS, Scanlon BR, Mpelasoka FS, C. R, Reedy RC, Gates JB, Zhang L. 2013b. Potential climate change effects on groundwater recharge in the High Plains Aqui-fer, USA. *Water Resource Research* **49**: 3936–3951
Daigneault R, Cousineau PA, Leduc E, Beaudoin G, Millette S, Horth N, Roy DW, Lamothe M, Allard G, Des 2011. Rapport final sur les travaux de cartographie, et al.

2011. *Rapport final sur les travaux de cartographie des formations superficielles réalisés dans le territoire municipalisé du Saguenay-Lac-Saint-Jean*. Ministère des Ressources naturelles et de la Faune du Québec, Canada.

Desbiens S, Lesperance PJ. 1989. Stratigraphy of the Ordovician of the Lac Saint-Jean and Chicoutimi outliers, Quebec. *Canadian Journal of Earth Sciences* **26**: 1185–1202

Deshmukh DS, Chaube UC, Ekube Hailu A, Aberra Gudeta D, Tegene Kassa M. 2013. Estimation and comparision of curve numbers based on dynamic land use land cover change, observed rainfall-runoff data and land slope. *Journal of Hydrology* **492**: 89–101

Dessureault R. 1975. *Hydrogéologie du Lac Saint-Jean, partie nord-est*. Ministère des richesses naturelles du Québec, Direction générale des eaux, Service des eaux souterraines.

Dionne FL, Ciobanas AI, Rousseau AN. 2008. *Validation d'un modèle de rayonnement net et comparaison de l'équation d'évaporation d'Hydro-Québec avec le bilan d'énergie thermique de surface*. INRS-Eau, Terre et Environnement, Rapport de recherche No R-1036.

Dionne JC, Laverdière C. 1969. Sites fossilifères du golfe de Laflamme. *Revue de géographie de Montréal* **23**: 259–270

Dubois E, Larocque M, Gagné S, Meyzonnat G. 2021. Simulation of long-term spatiotemporal variations in regional-scale groundwater recharge: Contributions of a water budget approach in southern Quebec. *Hydrology and Earth System Sciences* DOI: https://doi.org/10.5194/hess-2021-71

Engman ET, Gurney RJ. 1991. *Remote Sensing in Hydrology*. Chapman and Hall, London.

Epting J, Michel A, Affolter A, Huggenberger P. 2021. Climate change effects on groundwater recharge and temperatures in Swiss alluvial aquifers. *Journal of Hydrology* **11** (100071): 1–18

ESRI (Environmental Systems Research Institute). 2019. *ArcGIS Version 10.7.1*. www. arcgis.com.

Ferroud A, Chesnaux R, Rafini S. 2018. Insights on pumping well interpretation from flow dimension analysis: The learnings of a multi-context field database. *Journal of Hydrology* **556**: 449–474

Ferroud A, Chesnaux R, Rafini S. 2019. Drawdown log-derived analysis for interpreting constant-rate pumping tests in inclined substratum aquifers. *Hydrogeology Journal* **27** (6): 2279–2297

Flint LE, Flint AL. 2014. *California Basin Characterization Model: A Dataset of Historical and Future Hydrologic Response to Climate Change*. U.S. Geological Survey Data Release. doi: http://dx.doi.org/10.5066/F76T0JPB.

Fortin JP, Duchesne S, Bernier M, Huang KH, Villeneuve JP. 2007. HYDROTEL, un modèle hydrologique distribué pouvant générer des informations spatialisées détaillées très utiles pour la gestion de bassins versants de tailles diverses. In *Actes Des Journées Scientifiques Inter-Réseaux de l'Agence Universitaire de La Francophonie, Hanoi, Viet Nam, November, 6-7*.

Fortin JP, Moussa R, Bocquillon C, Villeneuve JP. 1995. Hydrotel, un modèle hydrologique distribué pouvant bénéficier des données fournies par la télédétection et les systèmes d'information géographique. *Revue des sciences de l'eau* **8** (1): 97–124

Galvão P, Hirata R, Conicelli B. 2018. Estimating groundwater recharge using GIS-based distributed water balance model in an environmental protection area in the city of Sete Lagoas (MG), Brazil. *Environmental Earth Sciences* **77** (398): 1–19

El Garouani A, Aharik K, El Garouani S. 2020. Water balance assessment using remote sensing, Wet-Spass model, CN-SCS, and GIS for water resources management in Saïss Plain (Morocco). *Arabian Journal of Geosciences* **13** (738): 1–9

Gassman PW, Reyes MR, Green CH, Arnold JG. 2007. *The soil and water assessment tool: historical development, applications, and future research directions*. Center for Agricultural and Rural Development, Iowa State University.

Golkarian A, Rahmati O. 2018. Use of a maximum entropy model to identify the key factors that influence groundwater availability on the Gonabad Plain, Iran. *Environmental Earth Sciences* **77** (369)

Government of Canada. 2021. *Canada's national climate archive*. http://www.climate.weatheroffice.ec.gc.ca/climate_normals/ [consulted in July 2019].

Green TR, Taniguchi M, Kooi H, Gurdak JJ, Allen DM, Hiscock KM, Treidel H, Aureli A. 2011. Beneath the surface of global change: Impacts of climate change on groundwater. *Journal of Hydrology* **405** (3–4): 532–560

Halford KJ, Mayer GC. 2000. Problems associated with estimating ground water discharge and recharge from stream-discharge records. *Groundwater* **38** (3): 331–342

Hayashi M, Farrow CR. 2014. Watershed-scale response of groundwater recharge to inter-annual and inter-decadal variability in precipitation (Alberta, Canada). *Hydrogeology Journal* **22** (8): 1825–1839

Healy RW. 2010. *Estimating Groundwater Recharge*. Cambridge University Press, Cambridge.

Hébert C, Lacoste P. 1998. *Géologie de la région de Jonquière -Chicoutimi*. Rapport géologique no. RG 96- 08, Ministère des Ressources Naturelles du Québec, Canada.

Held IM, Soden BJ. 2006. Robust Responses of the Hydrological Cycle to Global Warming. *Journal of Climate* **19**: 5686–5699

Herrera-Pantoja M, Hiscock KM. 2008. The effects of climate change on potential groundwater recharge in Great Britain. *Hydrological Processes* **22** (1): 73–86

Holman IP, Allen DM, Cuthbert MO, Goderniaux P. 2012. Towards best practice for assessing the impacts of climate change on groundwater. *Hydrogeology Journal* **20**: 1–4

Huet M, Chesnaux R, Boucher MA, Poirier C. 2016. Comparing various approaches for assessing groundwater recharge at a regional scale in the Canadian Shield. *Hydrological Sciences Journal* **61** (12): 2267–2283

Jha MK, Chowdary VM, Chowdhury A. 2010. Groundwater assessment in Salboni Block, West Bengal (India) using remote sensing, geographical information system and multi-criteria decision analysis techniques. *Hydrogeology Journal* **18** (7): 1713–1728

Jha MK, Chowdhury A, Chowdary VM, Peiffer S. 2007. Groundwater management and development by integrated remote sensing and geographic information systems: Prospects and constraints. *Water Resources Management* **21** (2): 427–467

Jyrkama MI, Sykes JF. 2007. The impact of climate change on spatially varying groundwater recharge in the grand river watershed (Ontario). *Journal of Hydrology* **338**: 237–250

Kammoun S, Trabelsi R, Re V, Henchiri K, Zouari J. 2018. Groundwater quality

assessment in semi-arid regions using integrated approaches: the case of Grombalia aquifer (NE Tunisia). *Environmental Monitoring and Assessment* **190** (87): 1–22
Kendall MG. 1975. *Rank Correlation Method*. Charless Griffin, London.
Labrecque G, Chesnaux R, Boucher MA. 2020. Water-table fluctuation method for assessing aquifer recharge: application to Canadian aquifers and comparison with other methods. *Hydrogeology Journal* **28**: 521–533
Lasalle P, Tremblay G. 1978. *Dépôts meubles du Saguenay Lac Saint-Jean. Rapport géologique n° 191, ministère des Richesses naturelles du Québec, Canada*.
Laurin AF, Sharma KNM. 1975. *Mistassini, Peribonka, Saguenay Rivers Area: Grenville 1965–1967*. Ministère des richesses naturelles, Direction générale des mines, Geological Exploration Service: Québec, QC, Canada.
Lentswe GB, Molwalefhe L. 2020. Delineation of potential groundwater recharge zones using analytic hierarchy process-guided GIS in the semi-arid Motloutse watershed, eastern Botswana. *Journal of Hydrology: Regional Studies* **28** (100674)
Lim KJ, Engel BA, Muthukrishnan S, Harbor J. 2006. Effects of initial abstraction and urbanization on estimated runoff using CN technology. *Journal of the American Water Resources Association* **42** (3): 629–643
Lindquist LW, Palmqutst KA, Jordan SE, Lauenroth WK. 2019. Impacts of climate change on groundwater recharge in Wyoming big sagebrush ecosystems are contingent on elevation. *Western North American Naturalist* **79** (1): 37–48
Mann HB. 1945. Nonparametric tests against trend. *Econometrica* **13**: 245–259
Meinken W, Stober I. 1997. Permeability distribution in the Quaternary of the Upper Rhine glacio-fluvial aquifer. *Terra Nova* **9** (3): 113–116
Meixner T, Manning AH, Stonestrom DA, Allen DM, Ajami H, Blasch KW, Brookfield AE, Castro CL, Clark JF, Gochis DJ, et al. 2016. Implications of projected climate change for groundwater recharge in the western United States. *Journal of Hydrology* **534**: 124–138
Miliani F, Ravazzani G, Mancini M. 2011. Adaptation of Precipitation Index for the Estimation of Antecedent Moisture Condition in Large Mountainous Basins. *Journal of Hydraulic Engineering* **16** (3): 218–227
Mohan C, Western AW, Wei YP, Saft M. 2018. Predicting groundwater recharge for varying land cover and climate conditions a global meta-study. *Hydrology and Earth System Sciences* **22** (5): 2689–2703
Monfet J. 1979. *Évaluation du coefficient de ruissellement à l'aide de la méthode SCS modifiée*. Gouvernement du Québec, ministère des Richesse naturelle: Service de l'hydrométrie.
Naghibi SA, Pourghasemi HR, Abbaspour K. 2018. A comparison between ten advanced and soft computing models for groundwater qanat potential assessment in Iran using R and GIS. *Theoretical and Applied Climatology* **131** (3–4): 967–984
Nampak H, Pradhan B, Manap MA. 2014. Application of GIS based data driven evidential belief function model to predict groundwater potential zonation. *Journal of Hydrology* **513**: 283–300
Ng GHC, McLaughlin D, Entekhabi D, Scanlon BR. 2010. Probabilistic analysis of the effects of climate change on groundwater recharge. *Water Resource Research* **46** (7): 1–18
Ogden FL, Hawkins RP, Walter MT, Goodrich DC. 2017. Comment on "beyond the SCS-

CN method: a theoretical framework for spatially lumped rainfall-runoff response" by M.S. Bartlett, et al. *Water Resource Research* **53** (7): 6345–6350
Oudin L. 2004. *Recherche d'un modèle d'évapotranspiration potentielle pertinent comme entrée d'un modèle pluie-débit global*. Ph.D thesis, ENGREF (AgroParisTech).
Ouranos. 2015. *Vers l'adaptation. Synthèse des connaissances sur les changements climatiques au Québec. Partie 1 : Évolution climatique au Québec*. Édition 2015, Montréal, Québec, Canada.
Parent M, Occhietti S. 1988. Late Wisconsinan Deglaciation and Champlain Sea Invasion in the St. Lawrence Valley, Québec. *Géographie physique et Quaternaire* **42**: 215–246
Parent M, Paradis SJ, Boivin R. 2010. *Formations superficielles, Légende et notes descriptives – 1/50 000 à 1/225 000, version 10*. Commission géologique du Canada, Bureau du Québec, Canada.
Pohlert T. 2020. *Non-Parametric Trend Tests and Change-Point Detection*. https ://creat iveco mmons .org/licen ses/by-nd/4.0/.
Poirier C, Fortier Fillion TC, Turcotte R, Lacombe P. 2014. *Reconstitution historique des apports verticaux (eaux de fonte et de pluie) de 1900 à 2010 – version 2012. Contribution au Programme d'acquisition de connaissances sur les eaux souterraines (PACES)*. Centre d'expertise hydrique du Québec (CEHQ), Direction de l'expertise hydrique, CEHQ, ISBN 978-2-550-71155-1, Québec, Canada.
Ponce VM, Hawkins RH. 1996. Runoff curve number: Has it reached maturity? *Journal of Hydrology* **1** (1): 11–19
Richard SK, Chesnaux R, Rouleau A. 2013. Detecting preferential seepage along casing installed in fractured rock aquifers: Examples from the Saguenay-Lac-Saint-Jean region, Canada. In *The 66th Canadian Geotechnical Conference and the 11th Joint CGS/IAH-CNC Groundwater Conference, September 29–October 3, 2013, Montreal, Quebec, Canada*.
Richard SK, Chesnaux R, Rouleau A. 2016a. Detecting a Defective Casing Seal at the Top of a Bedrock Aquifer. *Groundwater* **54** (2): 296–303
Richard SK, Chesnaux R, Rouleau A, Coupe RH. 2016b. Estimating the reliability of aquifer transmissivity values obtained from specific capacity tests: examples from the Saguenay-Lac-Saint-Jean aquifers, Canada. *Hydrological Sciences Journal* **61** (1): 173–185
Richard SK, Chesnaux R, Rouleau A, Morin R, Walter J, Rafini S. 2014. Field evidence of hydraulic connections between bedrock aquifers and overlying granular aquifers: examples from the Grenville Province of the Canadian Shield. *Hydrogeology Journal* **22** (8): 1889–1904
Rivard C, Paniconi C, Vigneault H, Chaumont D. 2014. A watershed-scale study of climate change impacts on groundwater recharge (Annapolis Valley, Nova Scotia, Canada). *Hydrological Sciences Journal* **59** (8): 1437–1456
Ross CW, Prihodko L, Anchang J, Kumar S, Ji W, Hanan NP. 2018. HYSOGs250m, global gridded hydrologic soil groups for curve-number-based runoff modeling. *Scientific Data* **5** (1): 1–9
Satheeshkumar S, Venkateswaran S, Kannan R. 2017. Rainfall–runoff estimation using SCS–CN and GIS approach in the Pappiredipatti watershed of the Vaniyar sub basin, South India. *Modeling Earth Systems and Environment* **3** (24): 1–8

Scanlon B, Healy RW, Cook PG. 2002. Choosing appropriate techniques for quantifying groundwater recharge. *Hydrogeology Journal* **10** (1): 18–39

Seddique AA, Masuda H, Anma R, Bhattacharya P, Yokoo Y, Shimizu Y. 2019. Hydrogeochemical and isotopic signatures for the identification of seawater intrusion in the paleobeach aquifer of Cox's Bazar city and its surrounding area, south-east Bangladesh. *Groundwater for Sustainable Development* **9** (100215): 1–12

Shultz D. 2020. More warming means worse impacts from runoff and drought. *Eos, Transactions American Geophysical Union* **101** DOI: doi.org/10.1029/2020EO145148

Steenhuis TS, Van Der Molen WH. 1986. The Thornthwaite-Mather procedure as a simple engineering method to predict recharge. *Journal of Hydrology* **84** (3–4): 221–229

Stephens DB. 2009. Also consider the recharge. *Groundwater* **47** (1): 2–3

Tanveer D, Nachiketa R, Aadil B. 2020. Delineation of potential groundwater recharge zones using analytical hierarchy process (AHP). *Geology, Ecology, and Landscapes*: 1–16

Taylor RG, Scanlon B, Döll P, Rodell M, Van Beek R, Wada Y, Longuevergne L, LeBlanc M, Famiglietti J, Edmunds M, et al. 2013. Ground water and climate change. *Nature Climate Change* **3**: 322–329

Tilahun K, Merkel BJ. 2009. Estimation of groundwater recharge using a GIS-based distributed water balance model in Dire Dawa, Ethiopia. *Hydrogeology Journal* **17**: 1443–1457

Turcotte R, Fortin LG, Fortin V, Fortin JP, Villeneuve JP. 2007. Operational analysis of the spatial distribution and the temporal evolution of the snowpack water equivalent in southern Québec, Canada. *Nordic Hydrology* **38** (3): 211–234

Wakode HB, Baier K, Jha R, Azzam R. 2018. Impact of urbanization on groundwater recharge and urban water balance for the city of Hyderabad, India. *International Soil and Water Conservation Research* **6** (1): 51–62

Walter J, Chesnaux R, Cloutier V, Gaboury D. 2017. The influence of water/rock − water/clay interactions and mixing in the salinization processes of groundwater. *Journal of Hydrology: Regional Studies* **13**: 168–188

Walter J, Chesnaux R, Gaboury D, Cloutier V. 2019. Subsampling of regional-scale database for improving multivariate analysis interpretation of groundwater chemical evolution and ion sources. *Geosciences (Switzerland)* **9** (139): 1–32

Walter J, Rouleau A, Chesnaux R, Lambert M, Daigneault R. 2018. Characterization of general and singular features of major aquifer systems in the Saguenay-Lac-Saint-Jean region. *Canadian Water Resources Journal* **43** (2): 75–91

Wanke H, Dunkeloh A, Udluft P, Wanke A. 2013. A distributed water balance model to esti-mate direct groundwater recharge: A case study from the Nhoma and Khaudum catchments, Namibia. *International Science and Technology Journal of Namibia* **2** (1): 11–32

Wieland M, Pittore M. 2017. A spatio-temporal building exposure database and information life-cycle management solution. *ISPRS International Journal of Geo-Information* **6 (4)** (114)

Woldeamlak ST, Batelaan O, De Smedt F. 2007. Effects of climate change on the groundwater system of the Grote-Nete catchment. *Hydrogeology Journal* **15** (5): 891–901

Woodward DE, Hawkins RH, Jiang R, Hjelmfelt AT, Van Mullem JA, Quan QD. 2003. Runoff curve number method: Examination of the initial abstraction ratio. In *In Proceedings of the World Water and Environmental Resources Congress and Related Symposis. American Society of Civil Engineers Publications, Philadelphia, PA. Vol. 10, No. 40685*.308.

Yeh HF, Lee CH, Chen JF, Chen WP. 2007. Estimation of groundwater recharge using water balance model. *Water Resources* **34** (2): 153–162

Yeh HF, Lin HI, Lee ST, Chang MH, Hsu KC, Lee CH. 2014. GIS and SBF for estimating groundwater recharge of a mountainous basin in the Wu River watershed, Taiwan. *Journal of Earth System Science* **123** (3): 503–516

Yuan Y, Nie W, Mccutcheon SC, Taguas EV. 2014. Initial abstraction and curve numbers for semiarid watersheds in Southeastern Arizona. *Hydrological Processes* **28** (3): 774–783

Zghibi A, Mirchi A, Msaddek MH, Merzougui A, Zouhri L, Taupin JD, Chekirbane A, Chenini I, Tarhouni J. 2020. Using analytical hierarchy process and multi-influencing factors to map groundwater recharge zones in a semi-arid mediterranean coastal aquifer. *Water (Switzerland)* **12** (9): 1–27

Zhang L, Dawes WR, Walker GR. 2001. Response of mean annual evapotranspiration to vegetation changes at catchment scale. *Water Resources Research* **37** (3): 701–708

Zomlot Z, Verbeiren B, Huysmans M, Batelaan O. 2015. Spatial distribution of groundwater recharge and base flow: Assessment of controlling factors. *Journal of Hydrology: Regional Studies* **4** (Part B): 349–368

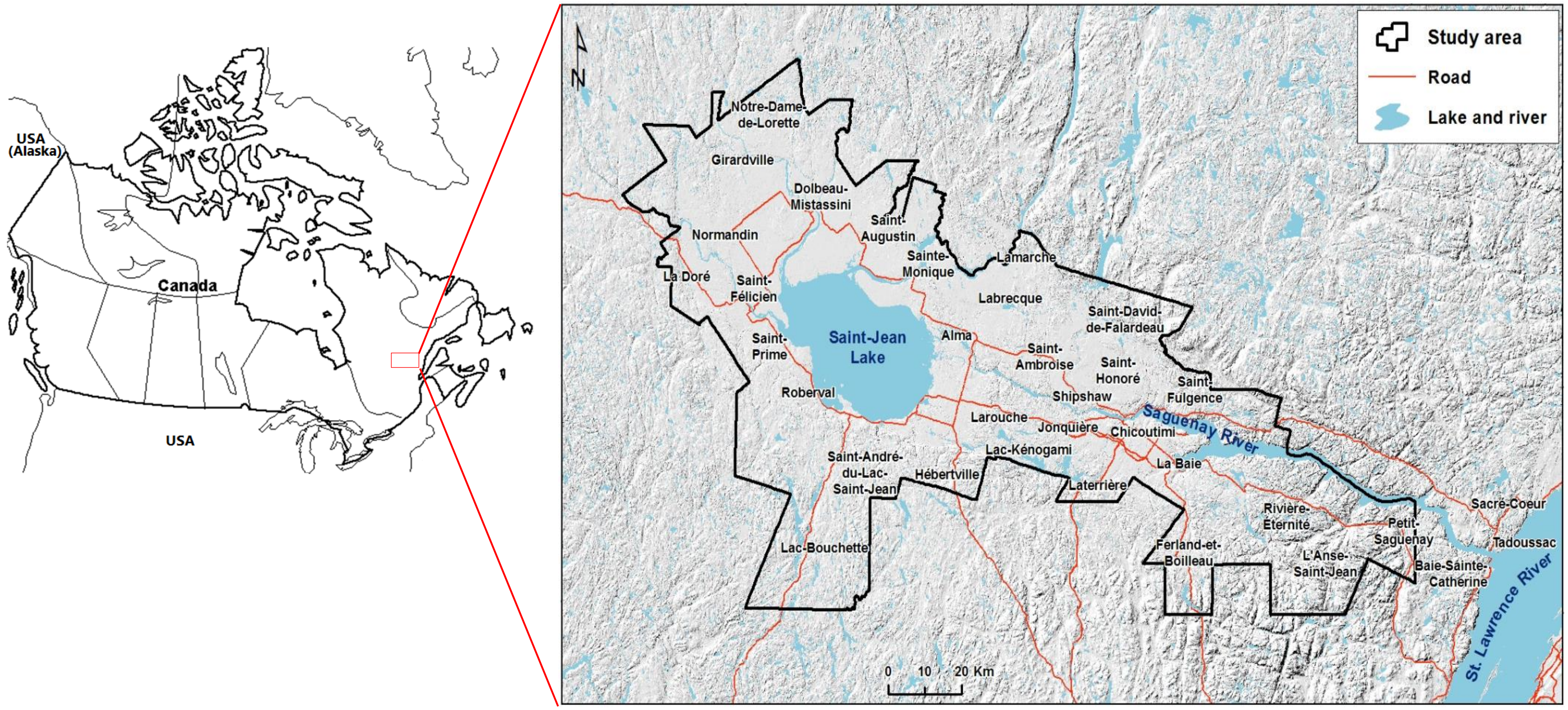

Figure 1. Geographic location of the study area and its administrative limits corresponding to territory administered by the municipalities belonging to the SLSJ region.

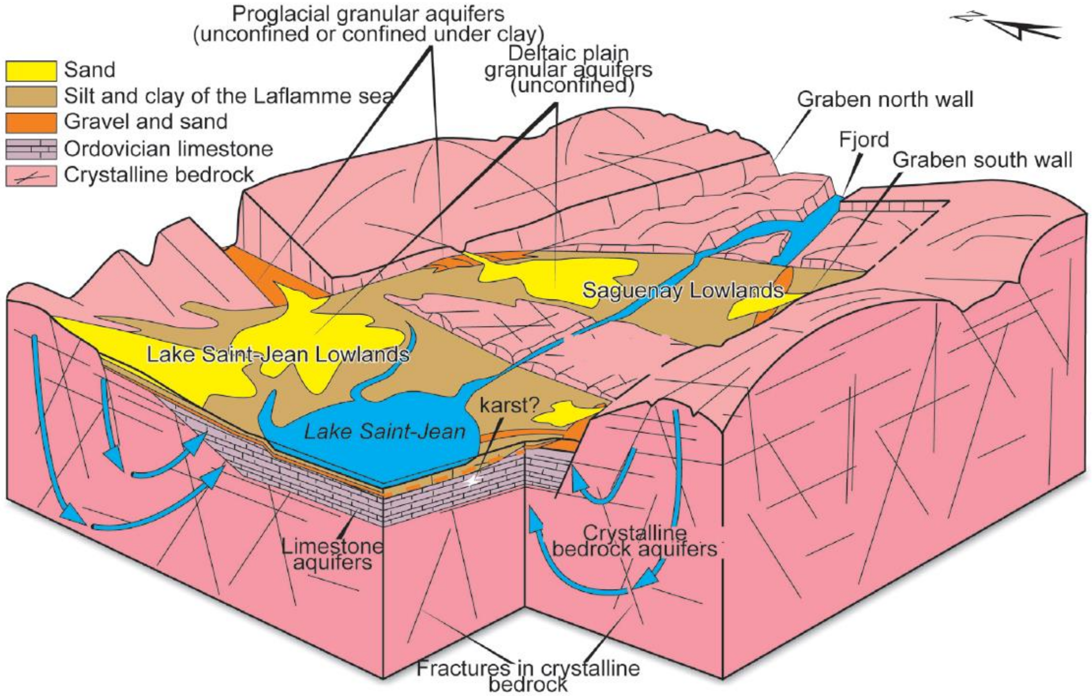
Proglacial granular aquifers
(unconfined or confined under clay)
Sand
Silt and clay of the Laflamme sea
Gravel and sand
Ordovician limestone
Crystalline bedrock
Deltaic plain
granular aquifers
(unconfined)
Graben north wall
Fjord
Graben south wall
Saguenay Lowlands
Lake Saint-Jean Lowlands
karst?
Lake Saint-Jean
Limestone
aquifers
Crystalline
bedrock aquifers
Fractures in crystalline
bedrock

(a)

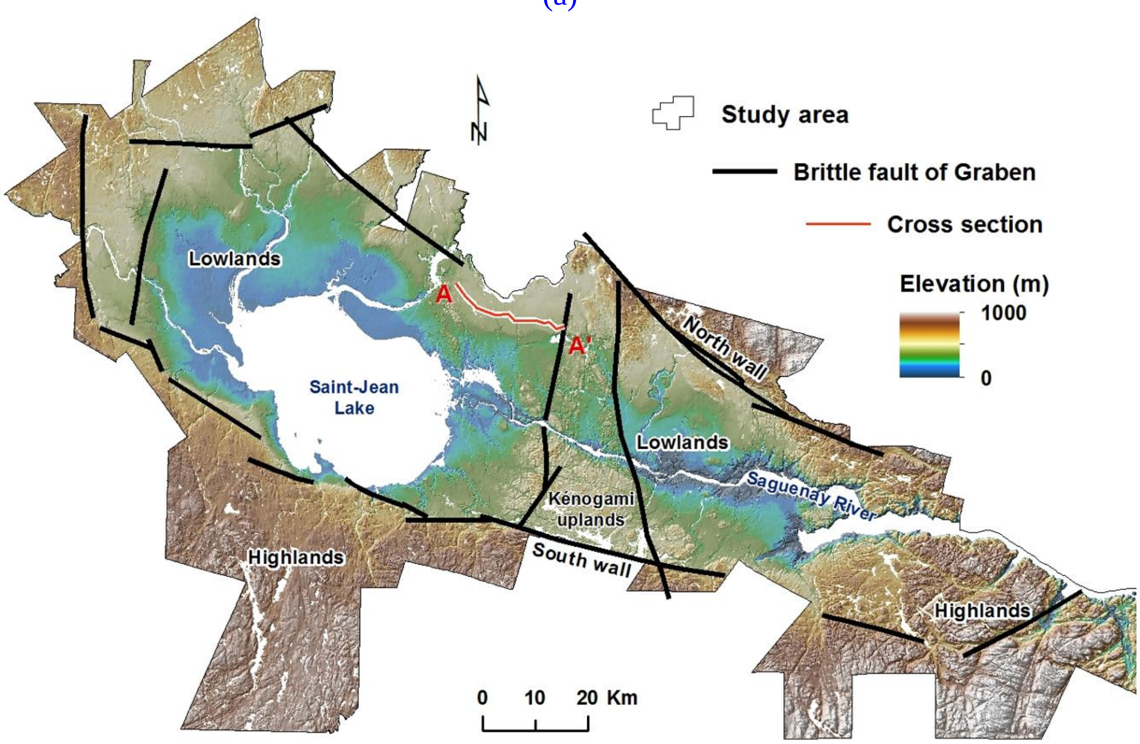
Study area
Brittle fault of Graben
Cross section
Elevation (m)
1000
0
N
Lowlands
A
A'
North wall
Saint-Jean
Lake
Lowlands
Saguenay River
Kénogami
uplands
Highlands
South wall
Highlands
0 10 20 Km

(b)

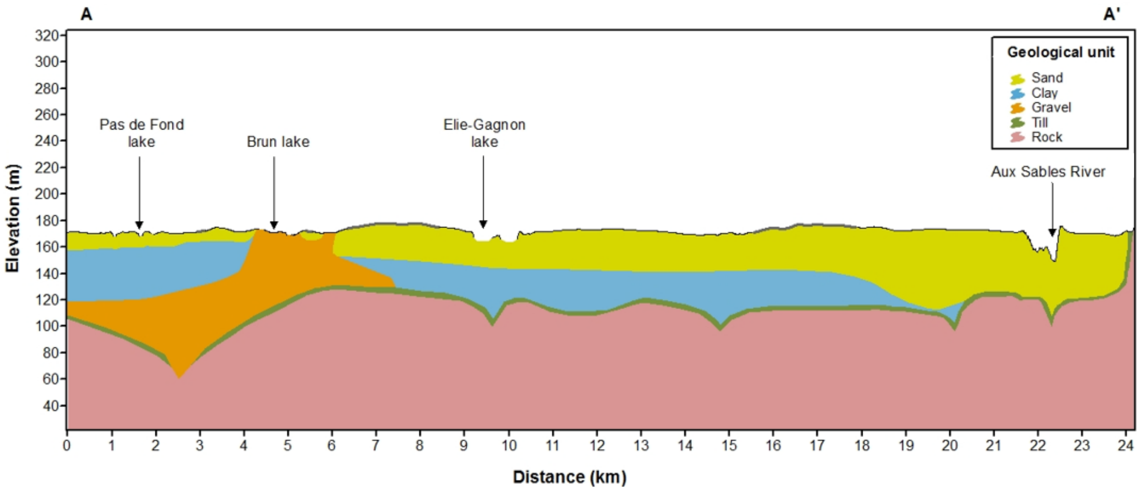

(c)

Figure 2. (a) Schematic block diagram of aquifer types identified in the SLSJ region; (b) Principal physiographic features of the SLSJ region, elevation is in meter above sea level; (c) Cross-section AA' – its location is indicated in Figure 2b (Adapted from CERM-PACES, 2013)

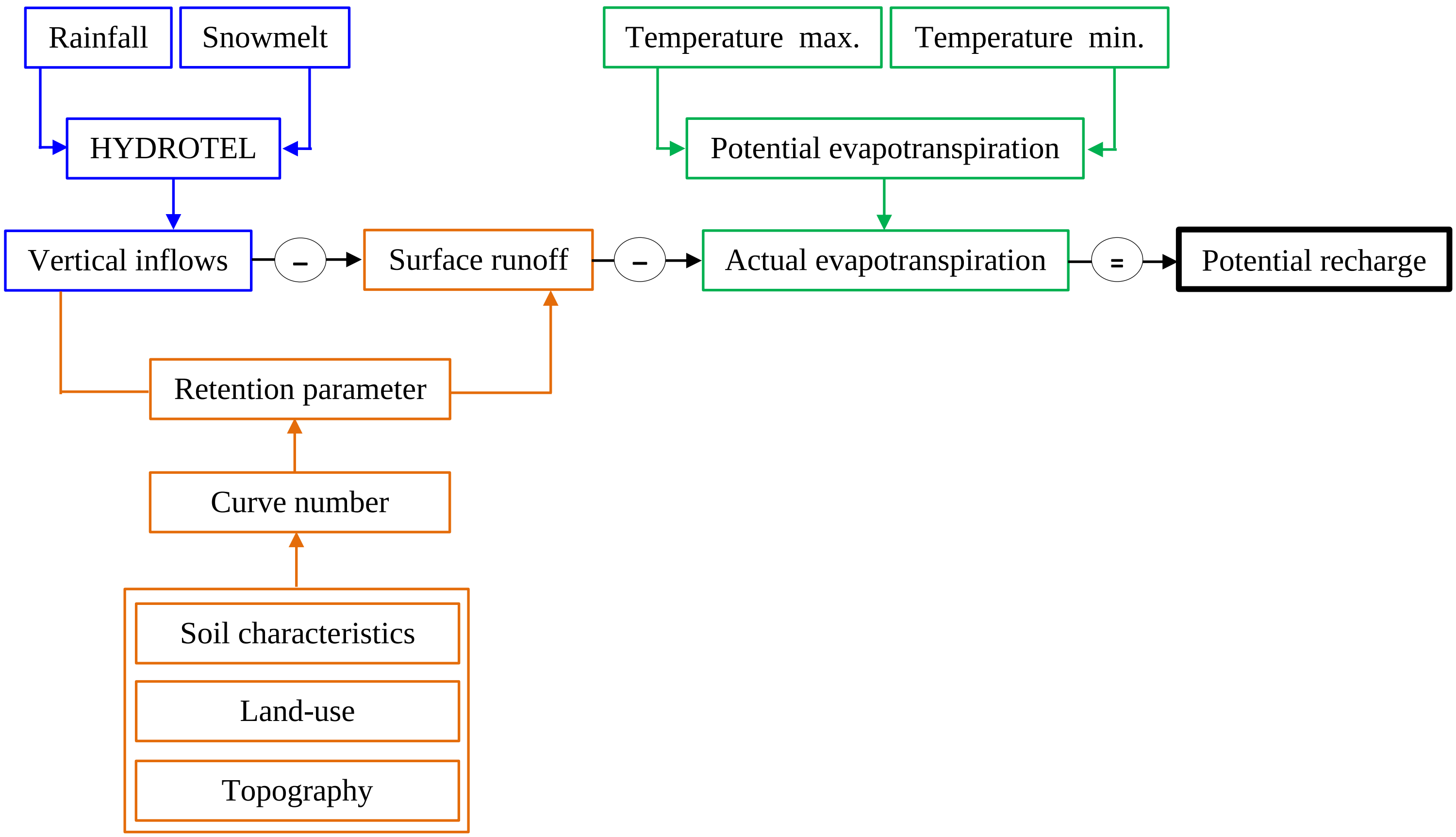

Figure 3. Procedure for computing the annual PGR using water budget method.

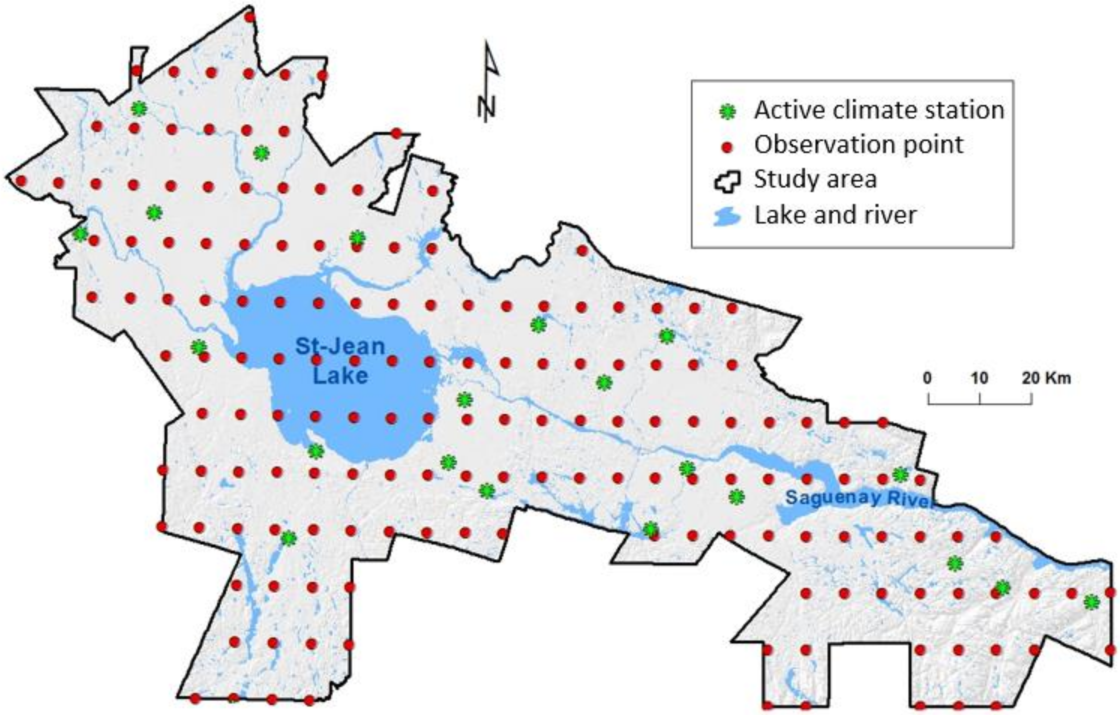

Figure 4. The distribution of the interpolated VI observation points over the SLSJ region.

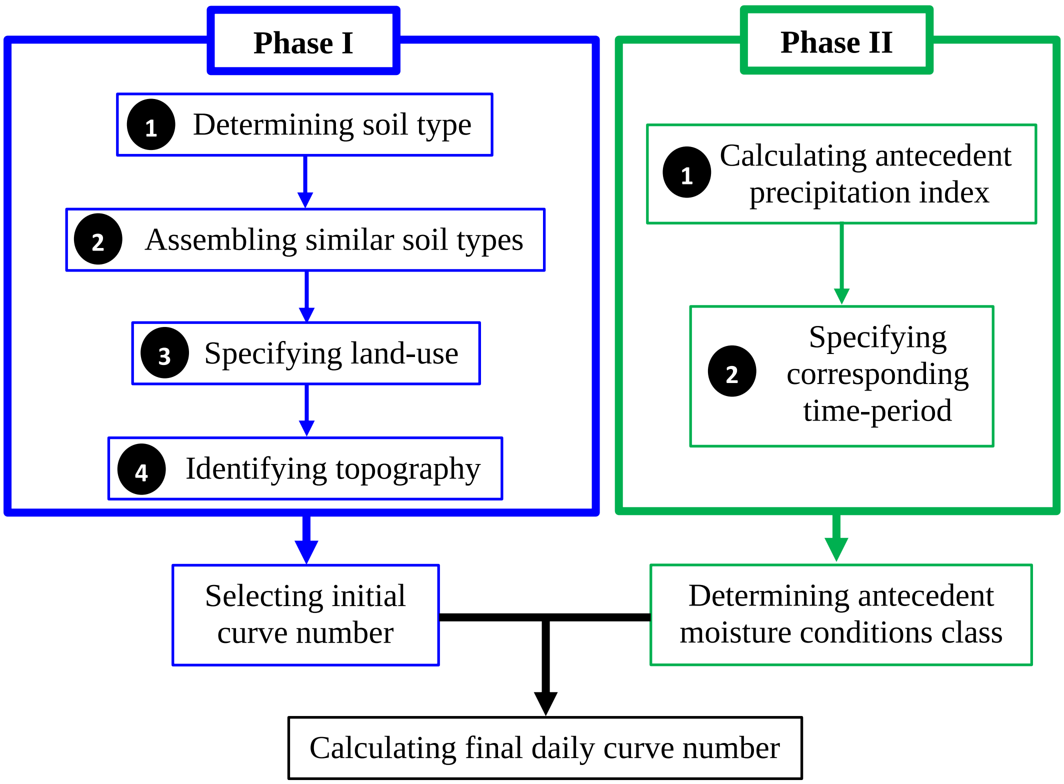

Figure 5. Steps to be followed for calculating daily curve number. Here, Phase I consists of determining the initial curve number (CN_i), whereas Phase II consists of determining the antecedent moisture conditions class.

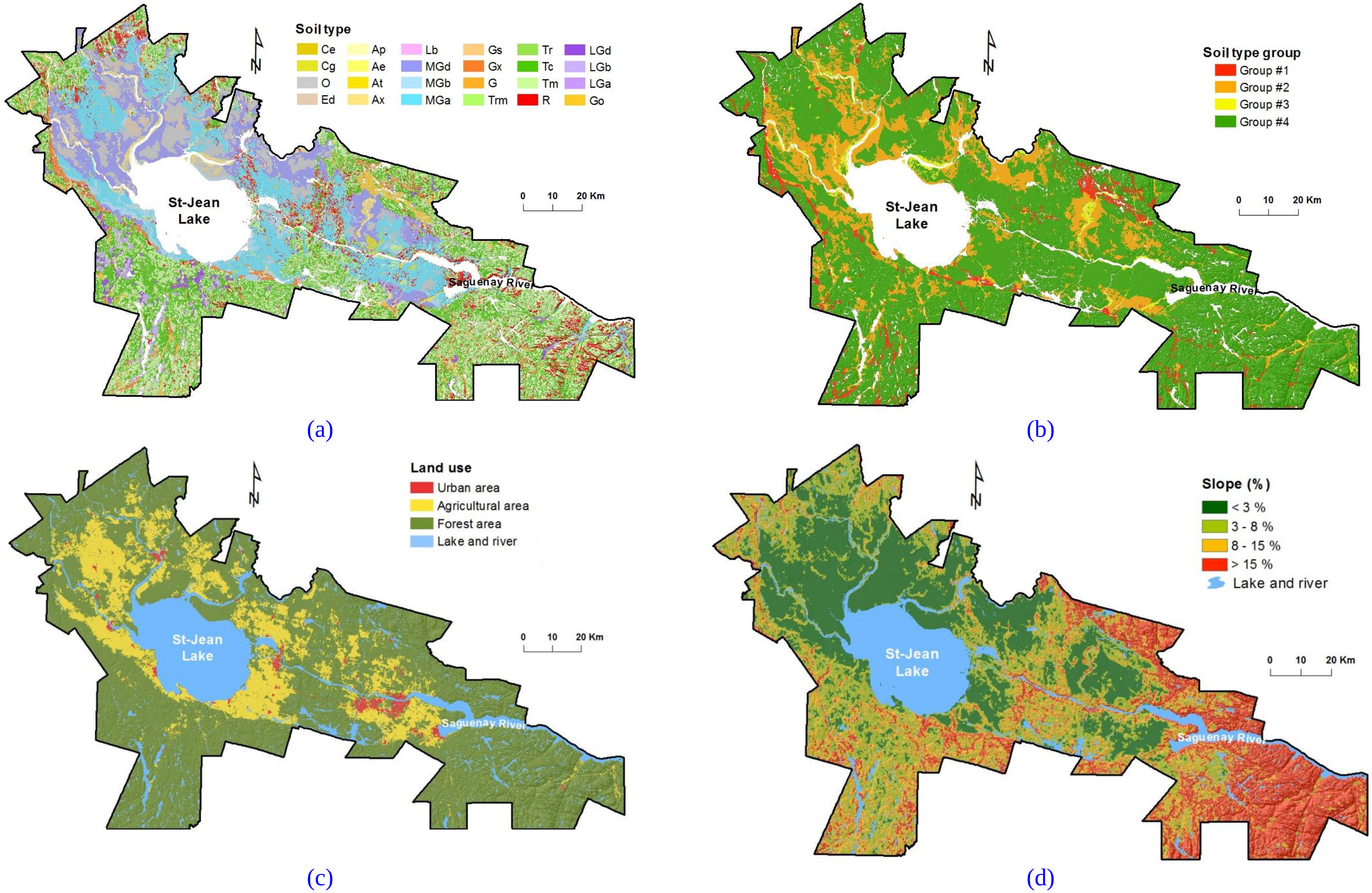

Figure 6. The thematic maps used to determine CNi: (a) soil types (see Table 1 for soil type code description), (b) soil type groups (see Table 2 for soil type group description), (c) land-use, and (d) terrain slope.

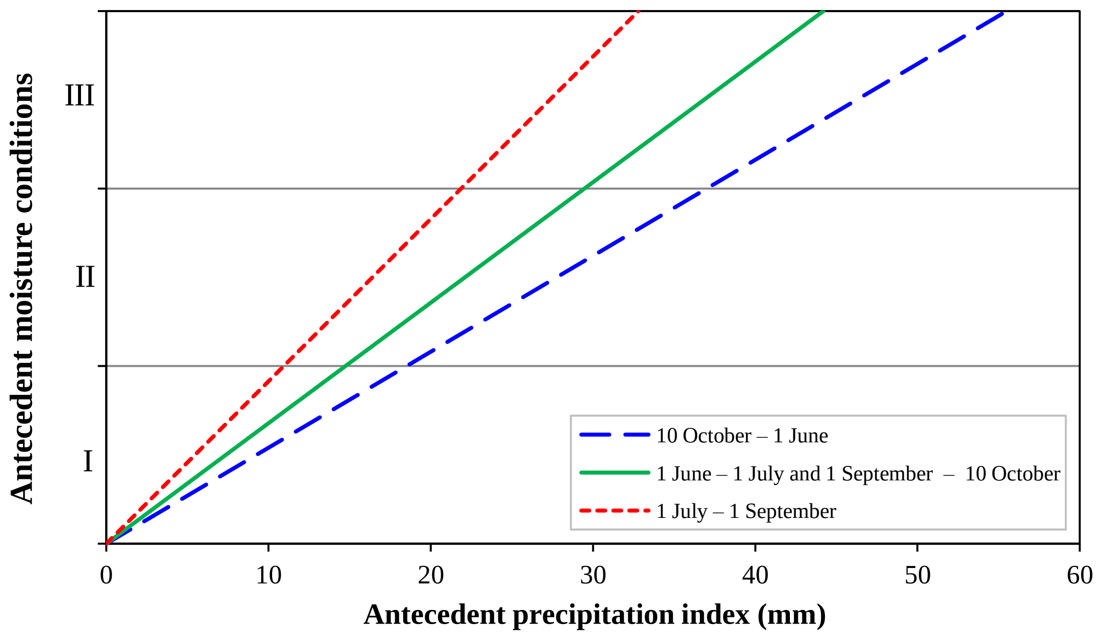

Figure 7. Chart for determining AMC class according to API and time-period (Adapted from Monfet (1979)).

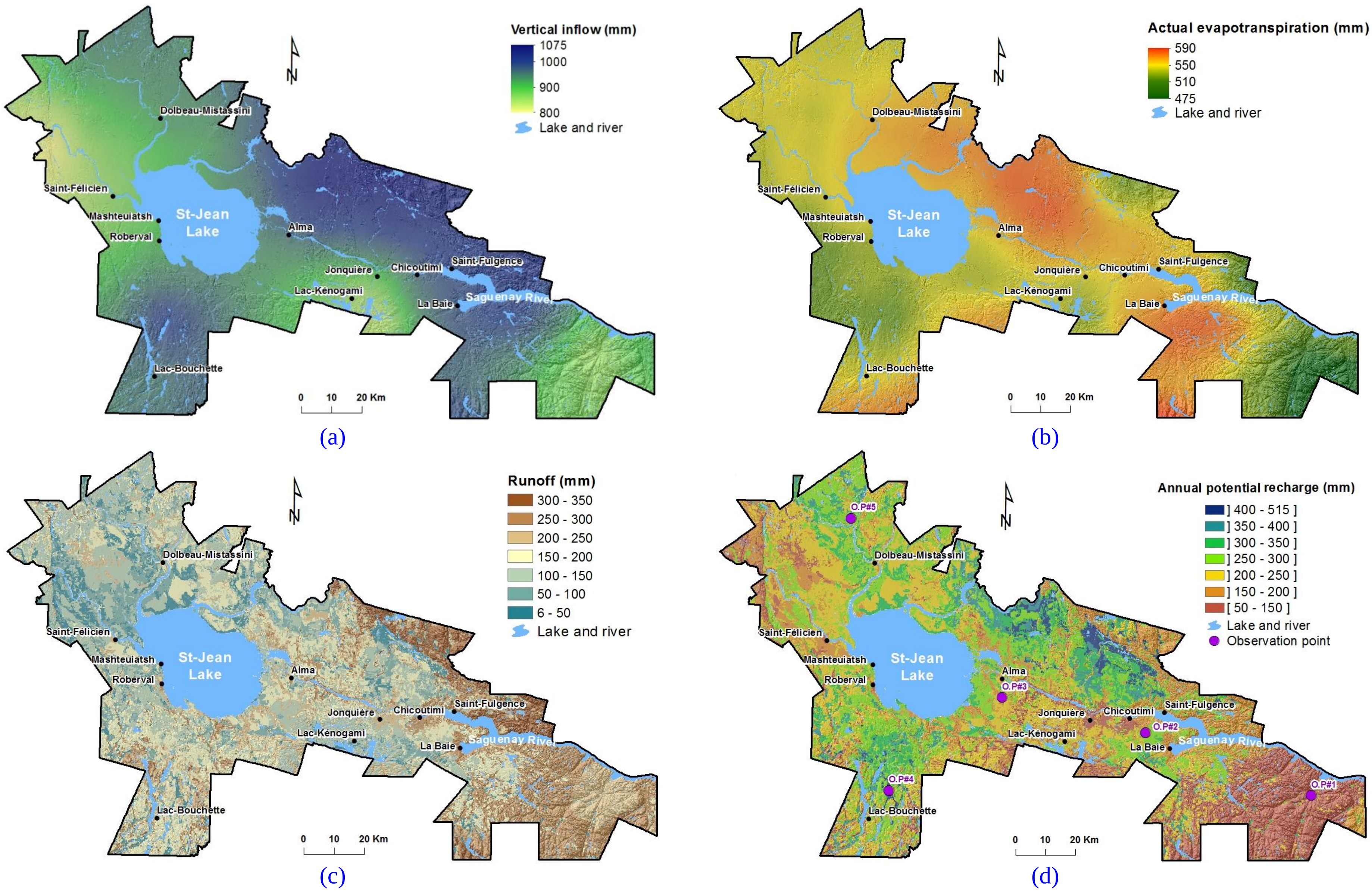

Figure 8. Spatial variation of the mean annual of (a) VI, (b) AET, (c) Ru_S, and (d) PGR during 2000–2009.

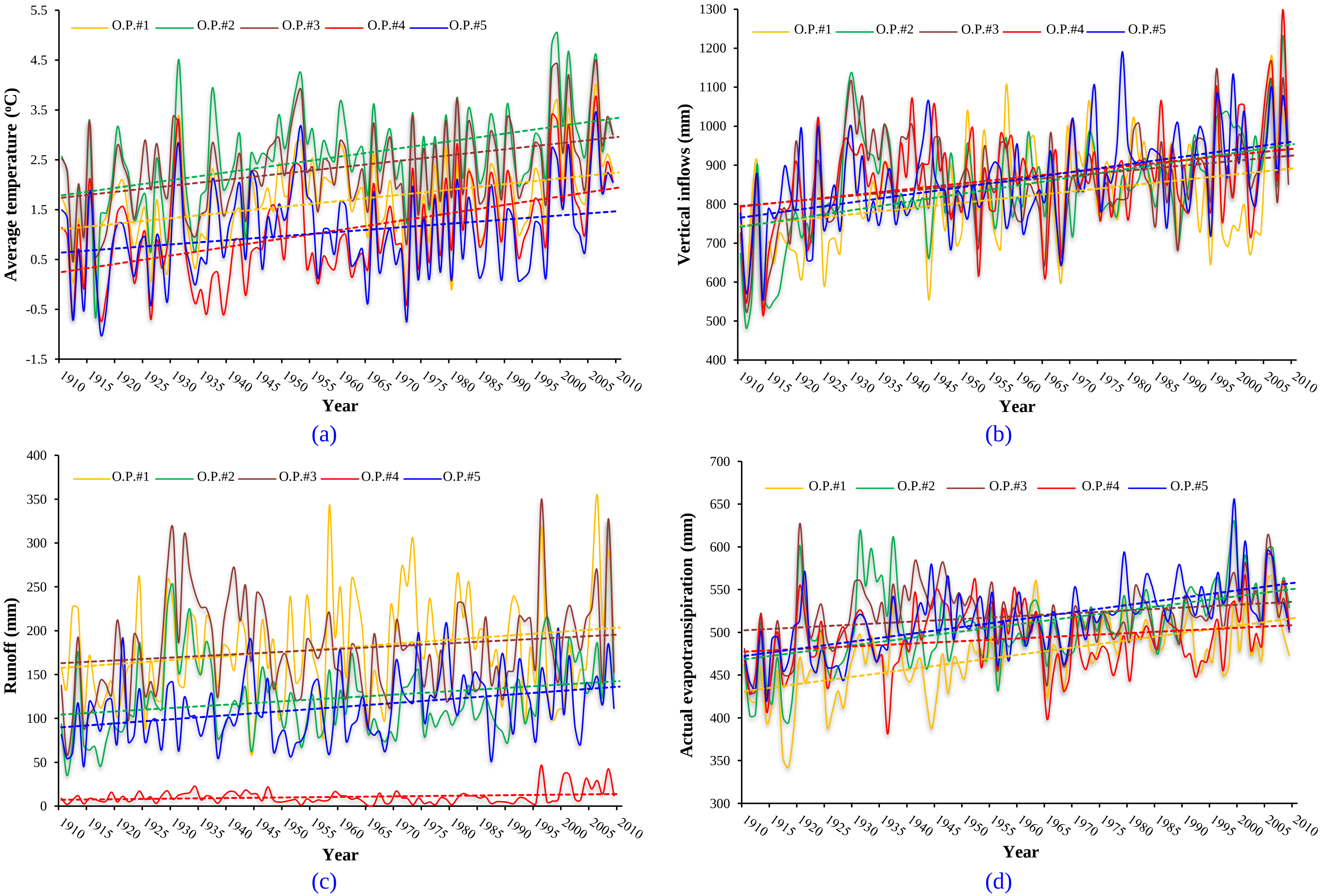

Figure 9. Temporal variations of (a) average temperatures, (b) VI, (c) Ru_S, and (d) AET for 1910–2009. Dashed lines represent the linear regression lines fit to data series.

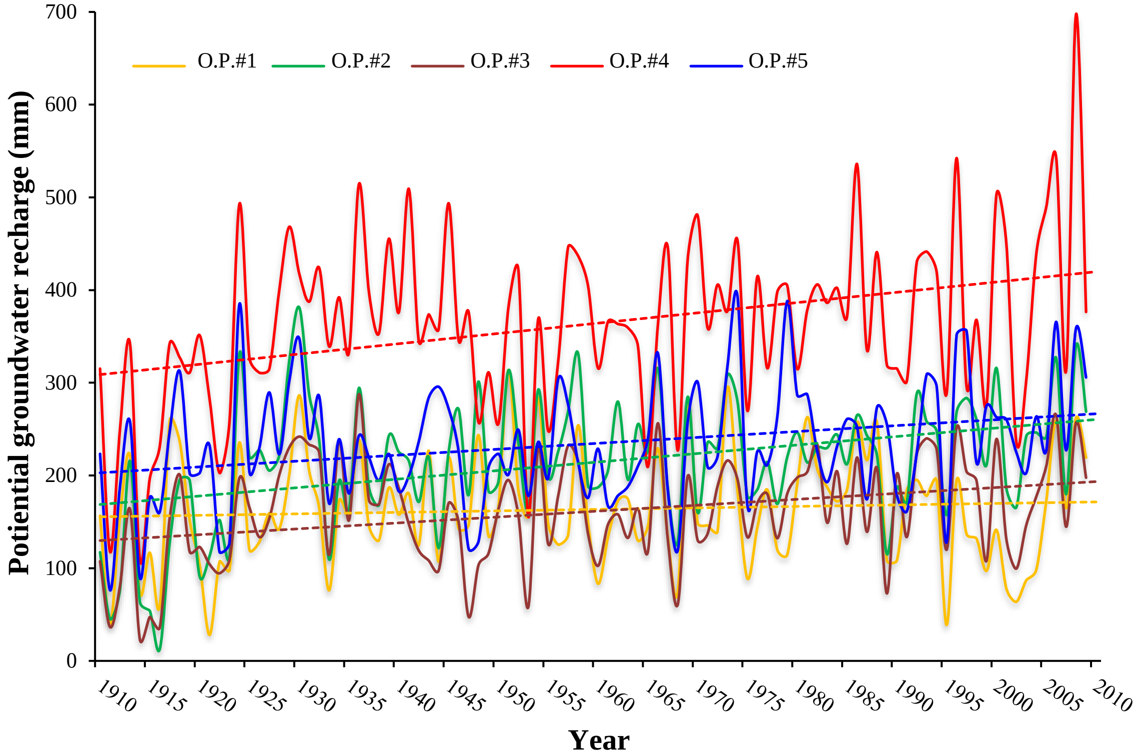

Figure 10. Temporal patterns of PGR for 1910–2009 (Dashed lines represent the linear regression lines fit to data series).

Table 1. Description of the main soil types observed in the SLSJ region

Description	**Code**
Alluvium sediments: Sand and sandy silt	Ap, Ax, Ae, At
Hillside deposits: Angular blocks, gravels with silt, and reorganized clay	Ce, Cg
Organic sediments	O
Glacier sediments: Discontinuous, continuous or fusion till	Tm, Tc, Trm, Tr
Glaciomarine: Gravels with silt, clay with silt	MGd, MGb, MGa
Glaciolacustrine sediments: Blocks with silt	LGb, LGd, LGa, Lb, Ed
Glaciofluvial sediments: Sandy, gravels and blocks	Go, Gx, G, Gs
Rock	R

Table 2. Assembled soil types according to their infiltration capacity

Code	**Group**
Go, Gx	1
Ce, MGb, MGd, LGb, LGd, Ed, Lb, G	2
Ax, Ap, At, Ae, Gs	3
Tm, Tc, Trm, Tr, R, O, Cg, MGa, LGa	4

Table 3. CNi values according to terrain characteristics (Adapted from Huet *et al.* (2016))

		Group of assembled soil			
		1	**2**	**3**	**4**
Land-use	**Slope (%)**	**CN_i**			
Agricultural area	< 3%	62	72	79	82
	3–8%	64	76	84	88
	8–15%	70	80	87	90
Forest area	< 3%	24	54	68	76
	3–8%	33	59	73	79
	8–15%	44	66	78	83
Urban area		73	83	88	90
Any area with slope >15%		90	90	90	90

Table 4. Statistical Mann-Kendall test results

		Observation points				
		O.P. #1	**O.P. #2**	**O.P. #3**	**O.P. #4**	**O.P.#5**
PGR	Kendall's Ʈ	0.389	0.391	0.130	0.139	0.468
	p-value	**<0.0001**	**<0.0001**	**0.05**	**0.04**	**<0.0001**
	A	0.05	0.05	0.05	0.05	0.05
	Trend	Increasing	Increasing	Increasing	Increasing	Increasing
Temp.	Kendall's Ʈ	0.265	0.303	0.255	0.340	0.147
	p-value	**<0.0001**	**<0.0001**	**0.000**	**<0.0001**	**0.030**
	A	0.050	0.050	0.050	0.050	0.050
	Trend	Increasing	Increasing	Increasing	Increasing	Increasing
VI	Kendall's Ʈ	0.223	0.320	0.178	0.189	0.340
	p-value	**0.001**	**<0.0001**	**0.009**	**0.005**	**<0.0001**
	A	0.05	0.05	0.05	0.05	0.05
	Trend	Increasing	Increasing	Increasing	Increasing	Increasing
AET	Kendall's Ʈ	0.398	0.391	0.130	0.139	0.468
	p-value	**<0.0001**	**<0.0001**	**0.05**	**0.04**	**<0.0001**
	A	0.05	0.05	0.05	0.05	0.05
	Trend	Increasing	Increasing	Increasing	Increasing	Increasing
Ru_s	Kendall's Ʈ	0.137	0.182	0.105	0.021	0.252
	p-value	**0.044**	**0.007**	**0.121**	**0.755**	**0.000**
	A	0.05	0.05	0.05	0.05	0.05
	Trend	Increasing	Increasing	No significant	No significant	Increasing

0.044: *p-value less than the confidence level of α = 0.05 (i.e., there is trend)*
0.121: *p-value greater than the confidence level of α = 0.05 (i.e., there is no significant trend)*